2016

DRIVE SIGNAL DEVELOPMENT FOR THE THERMOACOUSTIC LOUDSPEAKER

Troy Bouman
Michigan Technological University, tmbouman@mtu.edu

DRIVE SIGNAL DEVELOPMENT FOR THE THERMOACOUSTIC LOUDSPEAKER

By

Troy M. Bouman

A REPORT

Submitted in partial fulfillment of the requirements for the degree of

MASTER OF SCIENCE

In Mechanical Engineering

MICHIGAN TECHNOLOGICAL UNIVERSITY

2016

This report has been approved in partial fulfillment of the requirements for the Degree of MASTER OF SCIENCE in Mechanical Engineering.

Department of Mechanical Engineering-Engineering Mechanics

Report Advisor: *Dr. Andrew R. Barnard*

Committee Member: *Dr. Jason R. Blough*

Committee Member: *Christopher Plummer*

Committee Member: *Charles D. Van Karsen*

Department Chair: *Dr. William W. Predebon*

To my wife and family who have always supported me in my educational endeavors.

Table of Contents

List of Figures

List of Tables

Preface

A large portion of this work was accepted into The Journal of the Acoustical Society of America[1]. Specifically, all background, methods, results, discussion, and conclusions related to the signal processing techniques of alternating current (AC), direct current plus alternating current (DCAC) and amplitude modulation of an alternating current (AMAC) were accepted in a paper on February 15, 2016.

Acknowledgements

I would like to thank the contributions of so many who made my work possible. First, I would like to thank my advisor Dr. Andrew R. Barnard. Without his support not only would the project lack direction, but also successful implementation. Thank you to Professor Christopher N. Plummer, Professor Charles D. Van Karsen, and Dr. Jason R. Blough for agreeing to be on my committee and support me. Thank you to all of my lab and officemates, who provide great sounding boards when needed. Thank you Dr. Vesselin Shanov and your employees at NanoWorld Laboratories at the University of Cincinnati for growing the CNT forests. Thank you Stephania Vaglica for fabricating the CNT loudspeakers. Thank you Dr. Joshua Alexander from Purdue University for your assistance in understanding the time and frequency domain hearing aid algorithms. Thank you Steve Lehman for all of your assistance in setting up hardware and troubleshooting issues. Thank you Bill Langdon, Marty Toth, and Michael Goldsworthy for assistance in fabrication of the CNT fixture. Finally, I would like to acknowledge PCB Piezotronics® for their donation of the measurement microphones used in this effort.

List of Acronyms and Symbols

Acronyms

AC	Alternating Current
AMAC	Amplitude Modulation of an Alternating Current
ANSI	American National Standards Institute
B&K	Brüel & Kjær
CNT	Carbon Nanotube
CVD	Chemical Vapor Deposition
dB	Decibel
DC	Direct Current
DCAC	Direct Current added to Alternating Current
DI	Directivity Index
FCAC	Spectral Envelope Decimation
FGV	Functional Global Variable
IRB	Internal Review Board
MDF	Medium Density Fiberboard
MWNT	Multi-walled Nanotube
OTO	One Third Octave
PVC	Polyvinyl Chloride
SPL	Sound Pressure Level
STIPA	Speech Transmission Index for Public Address Systems
TCAC	Dynamic Linear Frequency Compression
TEG	Thermoelectric Generator
THD	Total Harmonic Distortion

Symbols

μ	Micro 10^{-6}	ρ_0	Density (kg/m^3)
p	Pico 10^{-12}	c	Speed of sound (m/s)
R^2	% Variation accounted for in model	c_p	Specific heat (J/(kg K))
η	True efficiency	T_a	Average temperature of thin film (K)
$\prod$	Acoustic power (watts)	T_0	Ambient temperature (K)
P_{input}	Electric power (watts)	β_0	Convection heat trans. coef. ($W/(m^2 K)$)
π	Pi 3.14159	S	Surface area (m^2)
f	Frequency (hertz)	A_M	Amplitude of modulated signal (volts)
B	DC offset (volts)	A_C	Amplitude of carrier signal (volts)
A	Signal amplitude (volts)	F_M	Frequency of modulated signal (hertz)
ω	Frequency (radians/second)	F_C	Frequency of carrier signal (hertz)
t	Time (seconds)	L_w	Sound power (decibels)
L_p	Sound pressure (decibels)	r	Radius (meters)

Abstract

Carbon nanotube thermophones can create acoustic waves from 1 Hz to 100 kHz. The thermoacoustic effect that allows for this non-vibrating sound source is naturally inefficient. Prior efforts have not explored their true efficiency (i.e. the ratio of the total acoustic power to the electrical input power). All previous works have used the ratio of sound pressure to input electrical power. A method for true power efficiency measurement is shown using a fully anechoic technique. True efficiency data are presented for five different drive signal processing techniques: standard alternating current (AC), direct current added to AC (DCAC), amplitude modulation of an AC signal (AMAC), spectral envelope decimation of an AC Signal (FCAC), and Dynamic Linear Frequency Compression of an AC signal (TCAC). These signal processing techniques are needed to limit the frequency doubling non-linear effects inherent to carbon nanotube thermophones. Each type of processing affects the true efficiency differently. Using a 72 Wrms input signal, the measured efficiency ranges were 4.3 E-6 - 319 E-6, 1.7 E-6 - 308 E-6, 1.2 E-6 - 228 E-6, 1.01 – 1083 E-6, and 1.26 – 388 E-6 percent for AC, DCAC, AMAC, FCAC, & TCAC, respectively. These data were measured in the frequency range of 100 Hz to 10 kHz. In addition, the effects of these processing techniques relative to sound quality are presented in terms of total harmonic distortion. It is shown that although the different signal processing techniques do affect the true efficiency, none of them will increase the efficiency of the CNT thermophone to the level of current moving coil loudspeakers. Future work optimizing the efficiency and ruggedness are needed.

1 Introduction

Carbon nanotube (CNT) thermophones create sound with heat, as opposed to a traditional moving coil loudspeaker, which uses a magnet to push and pull a metal coil of wire attached to a cone. This velocity boundary condition of a traditional speaker's cone creates the pressure wave that propagates to the listener's ear. In contrast, CNT thermophones use a thin-film that can oscillate its surface temperature at acoustic frequencies, creating a varying temperature boundary condition. With every heating cycle the air near the thin-film expands. When the current is removed from the thin-film, it cools, contracting the surrounding air. The repeated expansion and contraction of the adjacent air due to the thermal boundary condition creates the pressure wave that propagates to the listener's ear. This type of thermoacoustic device is called a thermophone.

The thermoacoustic effect was first published in 1898 by Braun, demonstrating how heat can create sound[2]. In the early 1900s, Arnold and Crandall explored this phenomenon using 700nm platinum, which could only heat and cool at frequencies less than 16 Hz, below the human audible range[3]. A material that could heat and cool quickly enough did not exist until 1991, when CNT thin-film was discovered[4]. In 2006, Yu et al. were the first to use the thermoacoustic effect with CNT thin-films and create sound in the audible range[5].

Carbon nanotubes have a very low heat capacity per unit area ($\sim 1 \times 10^{-4}$ J K^{-1})[6] and have been shown to oscillate their surface temperature at frequencies up to 100 kHz[7]. Without the heavy magnet of a traditional moving coil loudspeaker, CNT thermophones are useful for applications where a lightweight speaker is required. In addition, rare-earth metals, commonly used to reduce weight of traditional moving coil loudspeakers, are unnecessary. This makes CNT thermophones a good choice for sustainable loudspeakers. Application areas may include automotive, aerospace, and defense systems, where weight is at a premium. CNT thermophones are also flexible and stretchable, which allows them to be placed over complex geometric surfaces.

Several authors have analytically explored CNT thin-film thermophones[8-13]. Xiao et al., were the first to develop a theoretical model of the CNT thermophone's true efficiency, given as[14]

$$\eta = \frac{\Pi}{P_{input}} = \frac{\pi f^2 P_{input}}{2\rho_0 c C_P^2 (T_0 + T_a)^2} \quad , \tag{1}$$

where η is the efficiency, Π is the sound power (watts), P_{input} is the total input power (watts), f is the frequency (Hz), ρ_0 is the density of the surrounding gas (kg/m^3), c is the speed of sound in the surrounding gas (m/s), C_P is the specific heat of the surrounding gas (J/kg K), T_0 is the ambient temperature (K) of the surrounding gas, and T_a is the mean temperature (K) of the thin film. This model assumes the acoustic wavelength is much larger than the size of the source, i.e. it radiates as a monopole.

Prior to this effort, however, there has been minimal work measuring the efficiency of CNT thermophones[6,14,15]. Previous efficiency measurements compared the measured sound pressure level (SPL) at 1 meter to the total electrical input power into the CNT. However, in some experiments, the sound pressure level was not measured at 1 m, but instead measured in the nearfield (as close as 5 cm) and estimated at 1 m using spherical spreading. In addition, previous studies have focused on the low input power regime of CNT thermophones, on the order of 1 to 10 W_{rms}. True efficiency is defined as the ratio of acoustic output power (watts) to the input electrical power (watts). Experimentally measuring this true efficiency over a range of realistic input power levels is the initial goal of this work.

CNT thermophones are non-linear transducers. The non-linearity occurs because the output SPL is proportional to the square of the input electrical current. This causes a doubling of frequency between the input and output signals[12], resulting in significant distortion for broadband content

(e.g. speech, music, etc.). Signal processing techniques such as DC offset, amplitude modulation, and single-sided pulse width modulation have been shown to significantly reduce this distortion, but these methods require additional input power[6,11,16]. These processing techniques are used to modify the drive signal going into the CNT thermophone.

Because pressure is proportional to power (voltage or current squared), the AC input method produces a doubled output frequency. It is trivial to show this using the power reduction trigonometric identity. For the case of DCAC, this non-linearity results in an output pressure of

$$\mathrm{P(t)} \approx B^2 + 2BAsin(\omega t) + A^2[\tfrac{1-\cos(2\omega t)}{2}]. \quad (2)$$

where P is the pressure (pascals) as a function of time, t (seconds), A is the peak amplitude of the signal (volts), B is the amount of DC offset (volts), and ω is the frequency of the signal (rad/s). The doubled frequency is observed in the third term, the fundamental frequency appears in the second term, and the first term contributes to waste DC heating. For AMAC, the input voltage signal is

$$V(t) = \left(1 + A_M cos(2\pi F_M t)\right) * A_C \sin(2\pi F_C t), \quad (3)$$

which is squared due to the non-linearity of the system. In Eqn. (3), V is the voltage (volts) as a function of time, t (seconds), A_M is the amplitude of the modulated signal (volts), F_M is the frequency of the modulated signal (rad/s), A_C is the amplitude of the carrier signal (volts), and F_C is the frequency of the carrier (rad/s). The resulting components when this input signal is squared are F_M, $2F_M$, $2F_C$, $2F_C$-F_M, $2F_C$+F_M, $2F_C$+$2F_M$, and $2F_C$-$2F_M$. It is interesting to note the presence

of the $2F_M$ peak and second side lobes at $2F_C$+$2F_M$ and $2F_C$-$2F_M$, as these are not created in a linear loudspeaker's response to AMAC input.

The relative amplitudes of the modulated and carrier signal can also affect the response. This is typically described with Modulation Index, or the ratio of the modulated to carrier amplitude. Modulation depth is commonly used to describe modulation index as it is the percent representation of modulation index. For example, if a 1 Vpk 1000 Hz signal was modulated by a 2 Vpk 40 kHz carrier signal, the resulting signal would have a 0.5 modulation index or a 50% modulation depth.

Drawing from the hearing aid industry, different possible solutions for the frequency doubling issue were explored. Specifically, Dynamic Linear Frequency Compression[17], a time domain method, and spectral envelope decimation[18], a frequency domain method, allow the frequency content of a signal to be lowered by an octave. Dynamic Linear Frequency Compression was the first digital processing method used in hearing aids in 1991 by AVR Sonovation, a well known hearing aid manufacturer. It works by up sampling a signal by a factor of 2 and then low pass filtering the result. Spectral envelope decimation was first used in 2013. It takes a Fourier transform with 75% overlap, decimates the amplitude values by a factor of 2 with respect to frequency while not modifying the phase of each spectral line, and then inverse Fourier transforms to reconstruct the time domain signal.

This work will show a test method for measuring the true efficiency of thermophones and explore that efficiency using alternating current (AC), direct current offset with alternating current (DCAC), amplitude modulation of an alternating current (AMAC), spectral envelope decimation (FCAC), and Dynamic Linear Frequency Compression (TCAC).

Sound quality is also important for loudspeakers and can be a competing parameter with efficiency in thermophone design[9,10]. This work evaluates total harmonic distortion (THD) of the CNT thermophone as a function of many input parameters, such as frequency, the ratio of signal amplitude to amount of DC offset, the ratio of modulation frequency to carrier frequency, and modulation index. In this paper, THD is defined as the ratio of the sum total acoustical pressure of the 2-6th harmonics to the pressure of the fundamental, or

$$THD = \frac{Sum(pressure\ of\ 2{-}6th\ harmonics)}{pressure\ of\ fundamental}. \quad (4)$$

High THD results in an audio signal that is distorted and unintelligible. Therefore, the lowest possible THD as efficiency allows is desired for a high quality sound.

In the following sections, the testing methodology will be discussed. Then the efficiency results will be shown and discussed along with the THD results. Finally, the future work for the project will be discussed and outlined.

2 Methods

2.1 Carbon Nanotube Description

The CNT thermophones used for this work were composed of multi-walled nanotubes (MWNT) roughly 100 nm in length, grown on a silicon substrate. The CNT forests were grown by NanoWorld Laboratories at the University of Cincinnati using a chemical vapor deposition (CVD) technique[19-20]. These CNTs were grown in a forest and dry drawn over two copper rods by researchers at Michigan Tech. The CNT was not wrapped around the copper rods to prevent the formation of two sources, one on each side of the copper rod, creating cancelling pressure waves at high frequency. In order to ensure a good electrical connection, the CNT was densified onto the

copper rods using denatured alcohol. Two different thermophones were used for this work, but steps were taken to make them the same size. The thermophone in Figure 1 was used for the AC, DCAC, and AMAC data. Another thermophone was used for the FCAC and TCAC data. Structurally, each thermophone had six ribbons of CNT, each overlaid with five layers of thin-film, as shown in Figure 1. The total size was 9 cm high by 4.5 cm wide.

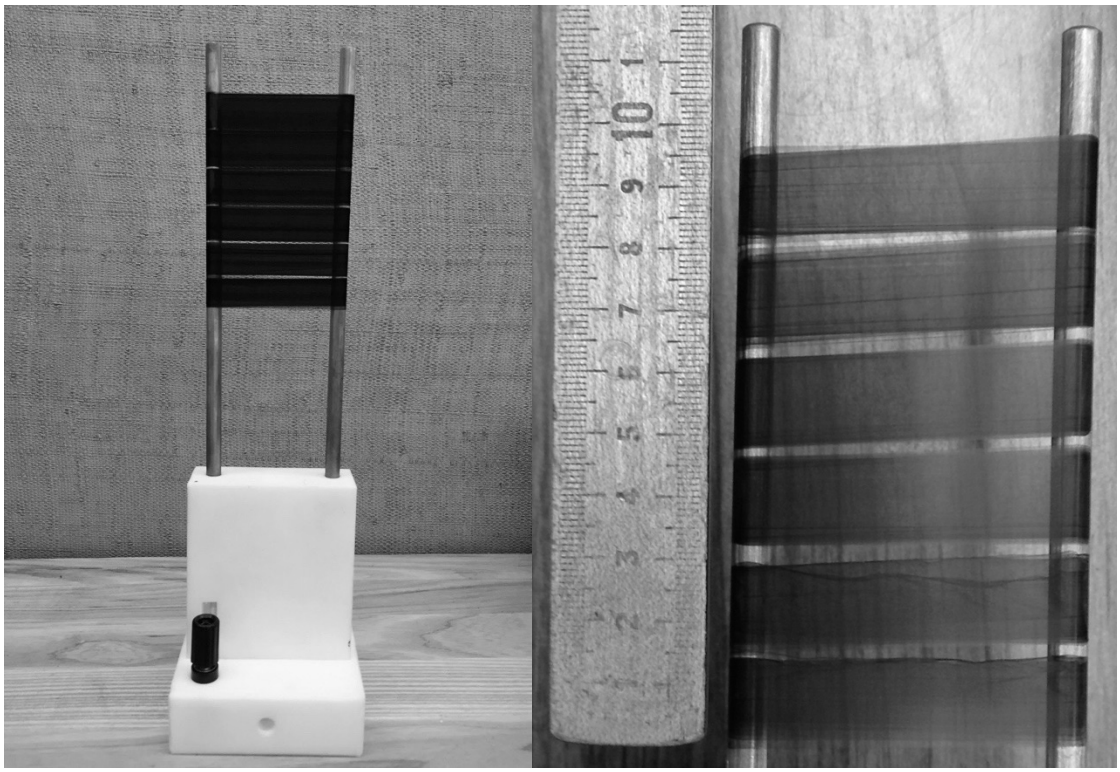

Figure 1: Picture of the CNT fixture used in this study (left) and a close up of the multiwalled CNT (right). Six ribbons, each five layers thick, were laid over two 101 copper rods. The CNT was not wrapped around the copper rods to prevent the formation of two sources, one on each side of the copper rod, creating cancelling pressure waves at high frequency.

2.2 Test Methology

To measure true efficiency, it was necessary to determine the acoustic power output and electrical power input to the CNT thermophone. ANSI S12.54 was used to measure the sound power level, which was then converted to watts of acoustic power using a reference power of 1 picowatt[21]. Per ANSI S12.54 sound power is calculated as[21]

$$L_w = \bar{L}_P - 10\log_{10}\frac{1}{2\pi r^2} - 10\log_{10}(\frac{\rho_0 c}{400}). \quad (5)$$

Where L_w is the sound power (dB re 20 pW), $\bar{L}_P$is the average sound pressure from all measurement locations (dB re 20 μPa), r is the radius of the hemisphere (m), ρ_0 is the density of area (kg/m^3), and c is the speed of sound in air (m/s).

The standard measurement was implemented in a fully anechoic chamber. The chamber has dimensions of 2.16 m long x 1.5 m wide x 2.16 m high. This limited the radius of a typical hemisphere to below 1 m, so the CNT thermophone was placed on a rotating table, controlled by a stepper motor, and four microphones were located in a 90° elevation arc at a radius of 1 meter from the CNT thermophone base as shown in Figure 2. Rotating the source in this configuration allowed for a 1 m radius measurement hemisphere. Data were acquired six times for each test with a 60 degree azimuth spacing to measure the entire hemisphere around the source. To illustrate the process at a single frequency: a sine wave was played through the CNT thermophone, data were then acquired simultaneously for five seconds (25 averages) at four elevation angles, the CNT thermophone was rotated 60 degrees in azimuth, data were again acquired, and this was repeated for six total azimuth locations. Once all of the locations had been recorded, a single sound power value was calculated. Because the input signal was a stationary sinusoid, the electrical power was found by measuring the time-averaged root-mean-square input voltage and current on the leads to the CNT thermophone. More details of the experimental setup are given in Appendix A.

For the AC, DCAC, FCAC, & TCAC signal processing techniques, PCB 130A23 microphones were used to measure sound pressure. Signal conditioning was provided internally from a National Instruments PXIe-4497 data acquisition (DAQ) module. For AMAC and THD measurements, PCB 378C01 high frequency microphones were used with external signal conditioners providing gain values of 100. All tests were conducted in air with a temperature range of 21-29 °C and

ambient pressure of 1014-1031 hPa. Ambient temperature and pressure were monitored throughout all testing to make the appropriate corrections when computing the sound power correction factor, per the standard.

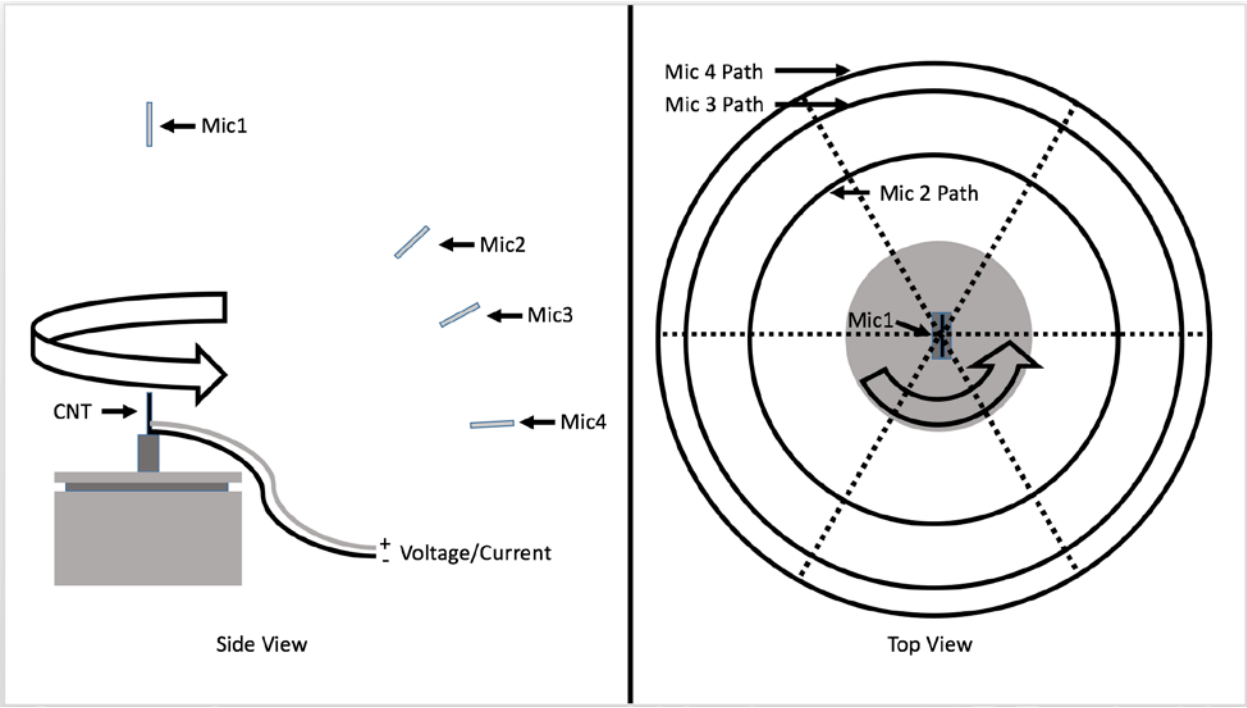

Figure 2: Test setup illustrating the implementation of ANSI S12.54 to measure average pressure around the CNT thermophone. Four elevation microphones took data at six azimuth locations (i.e. every 60 degrees-dashed lines) for each test.

Per ANSI S12.54, section 8.1.1b, if the source emits an A-weighted directivity index (DI) exceeding 5 dB in any direction, more microphones should be localized in that area. For example, the A-weighted DI in the elevation angle (i.e. between mic 4 and mic 1) is shown in Table 1. To account for this potential source of error, more microphones were localized in the area of high SPL for a single test. Figure 3 shows the standard 20 microphone locations for the ANSI S12.54 and the modified test locations. Due to testing time and equipment limitations, the modified test was only completed once and a sound power correction factor for each frequency was computed (Table 1). The correction factor was applied to all other data that were acquired with the standard locations shown in Figure 3. Because the source geometry and, therefore, its directivity were unchanged

throughout the testing, this correction process produced repeatable results, while minimizing testing time.

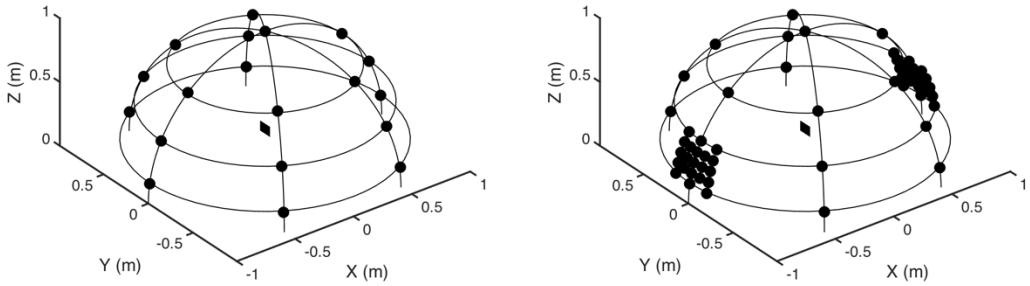

Figure 3: An isometric view of the standard 20 microphone locations outlined in ANSI S12.54 Annex B (left) and an isometric view showing the microphone locations used to compute the correction factor (right). The CNT thermophone is represented as a small square in the center of the hemisphere.

Table 1: Sound pressure level between microphone locations 4 and 1 for a total input power of 72 Wrms and the correction factor applied to all sound power results to correct for the error from the standard microphone locations in ANSI S12.54 while testing a directional source.

Low Frequency Region											
Frequency (Hz)	**100**	**125**	**160**	**200**	**250**	**315**	**400**	**500**	**630**	**800**	
SPL Difference (dBA re 20µPa)	-5.2	-3.6	-1.4	-2.3	-1.2	3.3	-1.1	-5.4	-1.5	2.3	
Lw Correction (dB re 1e-12W	-0.2	-0.2	-0.2	-0.2	-0.2	-0.3	-0.2	-0.1	-0.1	-0.2	
High Frequency Region											
Frequency (Hz)	**1k**	**1.25k**	**1.6 k**	**2k**	**2.5 k**	**3.15k**	**4k**	**5k**	**6.3 k**	**8k**	**10k**
SPL Difference (dBA re 20µPa)	1.3	3.8	5.2	6.6	8.5	17.1	32.4	28.1	28	26.4	29.9
Lw Correction (dB re 1e-12W	-0.1	-0.4	-0.4	0.3	0.3	0.4	0.7	-0.6	-0.6	-2.3	-1.8

To measure the input power, the same PXIe-4497 module was connected to a 111.5x attenuator to acquire voltage and a Fluke 80i-110s clamp-on current probe was used to measure current. Because CNT thermophones used in this study were not a pure resistors above 10 kHz (Figure 4), measuring the crosspower spectrum of these two signals allowed for easy computation of the true power (taking phase difference into account) at all frequencies. This series inductance was due to the parallel copper rods in the experimental setup. Figure 4 shows an example of the electrical impedance of the CNT thermophone used in this study.

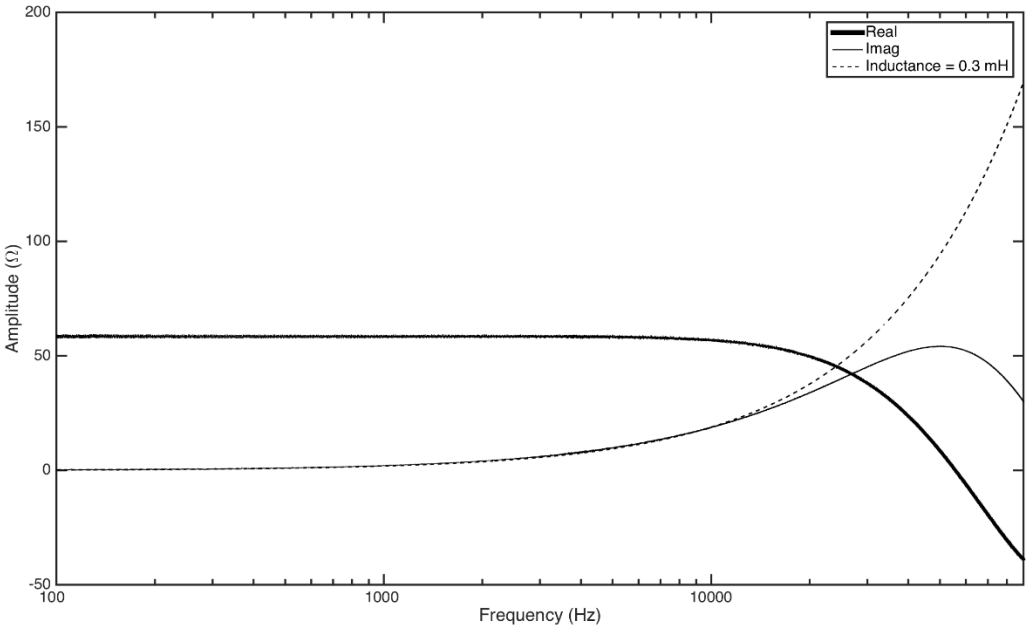

Figure 4: Impedance for the CNT thermophone used in this work showing the deviation from pure resistance above 10 kHz. Inductance plays an important role in the 10-20 kHz range, while a more complicated impedance model must exist at frequencies greater than 20 kHz. This complex impedance model is a function of the two parallel cooper rods used in this test (Figure 1). White noise 10 Hz to 100 kHz was played through the thermophone with total input power of 10 W_{rms}. 100 averages were taken and the resulting inductance was estimated at 0.3 mH for frequencies less than 20 kHz.

A LabVIEW code was written to run an automated ANSI S12.54 sound power test using a wav file input. The sound power level output and electrical input (watts) were stored. MATLAB was used to process the data. For the AC signal processing technique, data were obtained using pure sine wave inputs at one–third-octave (OTO) band center frequencies ranging from 100 Hz to 20

kHz. Frequency and total input power were varied, because these are the two most important independent variables in Xiao's efficiency equation (Eqn. (1))[14]. Since the sound pressure generated from CNT thermophones is proportional to the square of the input voltage signal, the efficiency for this signal processing technique was computed as the acoustic power (watts) in the second harmonic divided by the electrical input power in the fundamental,

$$AC\ Efficiency = \frac{Acoustic\ Power\ at\ The\ Second\ Harmonic}{Electrical\ Input\ Power\ at\ The\ Fundamenntal} * 100. \quad (6)$$

For DCAC, data were acquired at the same frequencies, but with varying amplitude ratios of DC current (*B*) to alternating current (*A*). These parameters were varied because of their influence in Eqn. (2). For the constant amplitude case, the AC amplitude (*A*) was unchanged and the DC amplitude (*B*) was varied to obtain different ratios of *B*/*A*. For the constant input power case, both *B* and *A* were manipulated to obtain different ratios of *B*/*A*, all with the same amount of total electrical input power to the CNT thermophone. The efficiency for DCAC was computed using

$$DCAC\ Eff. = \frac{Acoustic\ Power\ Out\ at\ the\ Fundamental}{Sum\ of\ Electrical\ Power\ Into\ The\ Fundamental\ and\ the\ DC\ offset} * 100\ . \quad (7)$$

For AMAC, data were acquired at the same frequencies but for varying ratios of the carrier frequency (F_c) to modulated frequency (F_m). The efficiency for AMAC was computed as

$$AMAC\ Efficiency = \frac{Acoustic\ Power\ Out\ at\ the\ Fundamental}{Sum\ Of\ All\ Power\ Into\ The\ CNT\ Thermophone} * 100, \quad (8)$$

noting that the denominator is the sum of all frequencies. Additionally, modulation depth was studied by looking at the effects of the ratio of the carrier signal amplitude (A_c) to the modulated signal amplitude (A_m).

For FCAC and TCAC, data were acquired at the same OTO frequencies. The efficiency was calculated using

$$FCAC\ \&\ TCAC\ Eff. = \frac{Acoustic\ Power\ Out\ at\ the\ Fundamental}{Electrical\ Input\ Power\ at\ Half\ The\ Fundamenetal} * 100. \quad (9)$$

The acoustic power is created at the fundamental, but the input electrical power is an octave below the fundamental. Therefore, the efficiency is the ratio of the fundamental acoustic response to the electrical input at half of the fundamental.

THD was not computed for the AC signal processing technique as no acoustic waves are produced at the fundamental. Thus THD is theoretically infinite for this processing technique (i.e. the denominator is approximately zero, to within the noise floor of the data acquisition system, for Eqn. (4)). THD was calculated for the DCAC, AMAC, FCAC, and TCAC using the 2nd-6th harmonics because there is no significant contribution to the total power from the higher harmonics.

3 Results and Discussion

The results from the low and high input power AC case are shown in Figure 5. The true efficiency of a CNT thermophone varies from 4.3 E-6 to 319 E-6 percent between 100 Hz and 10 kHz for 72 W_{rms} total input power. To get an idea of the SPL for a test, the level on-axis at 1m was 66.5 dB re 20 µPa for a 72 W_{rms} 1 kHz sine wave. This is theoretically the peak efficiency case, from a signal processing perspective, for this device at this input power, because all of the acoustic power in the second harmonic (i.e. the doubled frequency) is directly from the electrical power in the fundamental frequency with no signal processing. DCAC requires DC electrical power to shift the signal, AMAC requires high frequency electrical power to produce the carrier frequency, FCAC requires preprocessing of the signal, and TCAC also requires preprocessing, but FCAC and TCAC do not require additional input power. Therefore, DCAC and AMAC processing techniques were expected to decrease the efficiency of the thermophone, and FCAC and TCAC were expected to be similar to AC as they do not require additional power.

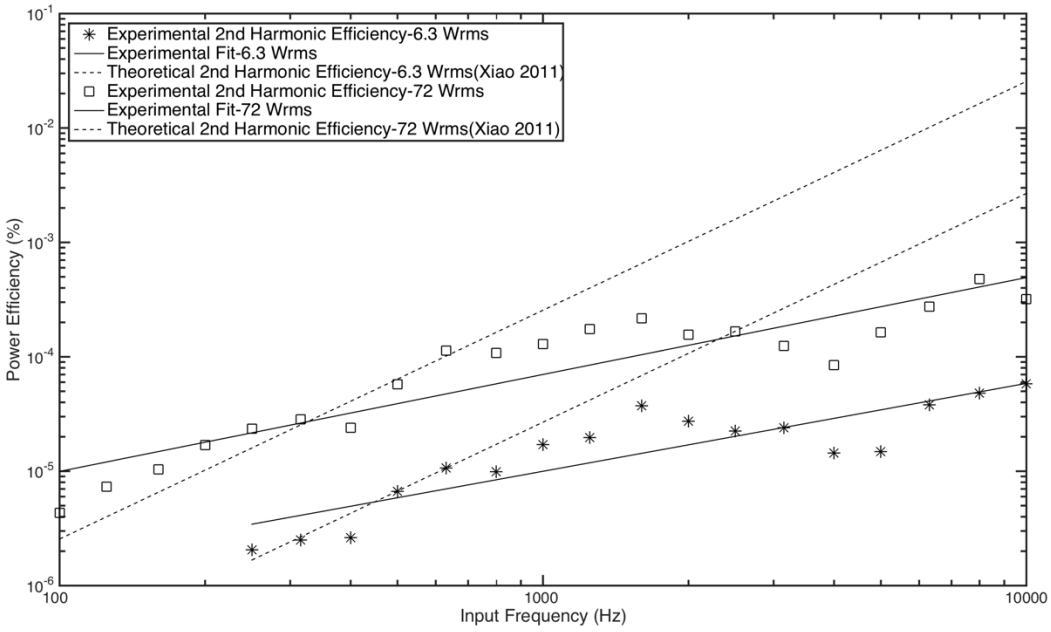

Figure 5: AC true efficiency data for total input power of 6.3 W_{rms} and 72 W_{rms}. This is the ratio of acoustic power generated in the second harmonic divided by the electrical power in the fundamental (Eqn. (6)). The resulting fit lines of the experimental data are

shown in Eqn. (10) & Eqn. (11). The experimental data is consistent with the theoretical model from Xiao (2011) for lower frequencies[14]. Note: the lower power 6.3 Wrms data was only taken from 250 to 10,000 Hz.

The power series fit for the AC case with 6.3 W_{rms} input power (Figure 5) is

$$Power\ Efficiency\ (\%) = 50\text{E} - 9 * f^{0.77}, \tag{10}$$

where f is the frequency in Hz and the percentage of the response variable variation that is explained by the model, R^2, is 76%. The power series fit for the AC case with 72 W_{rms} input power (Figure 5) is

$$Power\ Efficiency\ (\%) = 201\text{E} - 9 * f^{0.85} \tag{11}$$

and the R^2 value is 84%. The values used to compute the Xiao efficiency, from Eqn. (1), are shown in Table 2.

Table 2: Values used to compute the Xiao efficiency. Convective heat transfer coefficient, β_0, was obtained from Xiao et al. for a stack of 5 thin films as it was not obtained experimentally[14].

ρ_0 (kg/m^3)	c (m/s)	C_P (J/(kg K))	T_0 (K)	T_a (K)	β_0 (W/(m^2 K))	S (m^2)
1.1764	343	1.00643E3	297.15	$\frac{P_{input}}{2\beta_0 S}$	66	0.017

The experimental data agreed well with Eqn. (1) while the source radiated in a monopole-like pattern at frequencies below 1,600 Hz. At frequencies higher than 1,600 Hz, the height of the source, 9 cm, is large with respect to a wavelength and the source begins to become directional (Helmholtz number = 2.64). When comparing the two power level efficiencies in Figure 5 it was observed that increasing power increases efficiency, as expected from Eqn. (1).

A standard moving coil loudspeaker was tested as a baseline and the results are shown in

Table 3. The moving coil loudspeaker was a custom-made PVC pipe speaker with an Axon 6s1 6-1/2" Shielded Midbass, an Audax DTW100TI25 4 Ohm 1" Dome tweeter, and a crossover frequency of approximately 4 kHz[22] (Figure 6). Efficiency for this test was calculated using

$$Standard\ Efficiency = \frac{Acoustic\ Power\ Out\ at\ The\ Fundamental}{Electrical\ Power\ In\ The\ Fundamental} * 100. \quad (12)$$

Table 3: Efficiency & THD results for a standard moving coil loudspeaker. Efficiency was calculated using Eqn. (12). Total input power was 0.6 Wrms. THD was calculated with Eqn. (4).

Low Frequency Region											
Frequency (Hz)	**100**	**125**	**160**	**200**	**250**	**315**	**400**	**500**	**630**	**800**	
Efficiency (%)	0.41	0.38	0.38	0.27	0.23	0.31	0.32	0.39	0.45	0.67	
THD (%)	1.65	1.37	1.34	1.10	0.98	0.60	0.51	0.89	0.69	0.77	
High Frequency Region											
Frequency (Hz)	**1k**	**1.25k**	**1.6k**	**2k**	**2.5k**	**3.15k**	**4k**	**5k**	**6.3k**	**8k**	**10k**
Efficiency (%)	0.21	0.38	0.22	0.20	0.18	0.10	0.11	0.15	0.14	0.08	0.07
THD (%)	1.02	0.96	0.85	0.46	0.54	0.40	0.59	0.26	0.91	1.81	0.87

Figure 6: Custom moving coil loudspeaker (PVC speaker) used for efficiency and THD comparison.

The standard speaker had an efficiency ranging from 7 E-2 to 67 E-2 percent. In approximate terms, the CNT thermophone was four orders of magnitude less efficient than the traditional moving coil loudspeaker.

For the second signal processing technique, DCAC, Figure 7 and Figure 8 show the results for constant amplitude and constant input power, respectively.

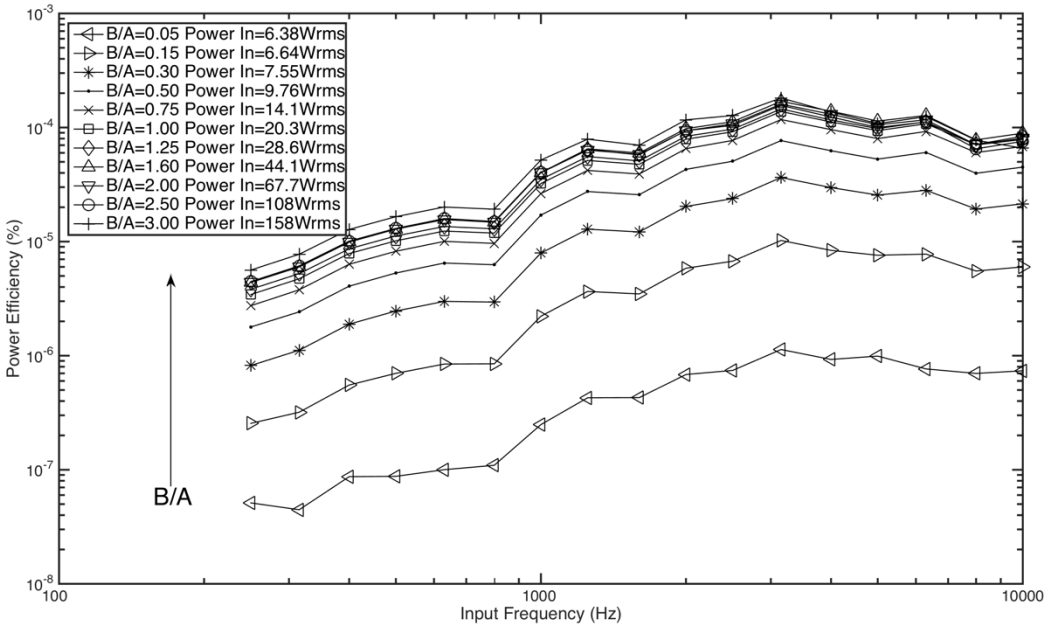

Figure 7: DCAC true efficiency data for a constant amplitude. The signal amplitude (A) was held constant while the amount of DC offset (B) was varied. Efficiency was computed with Eqn. (7). Efficiency is shown to increase significantly with increased power, as expected.

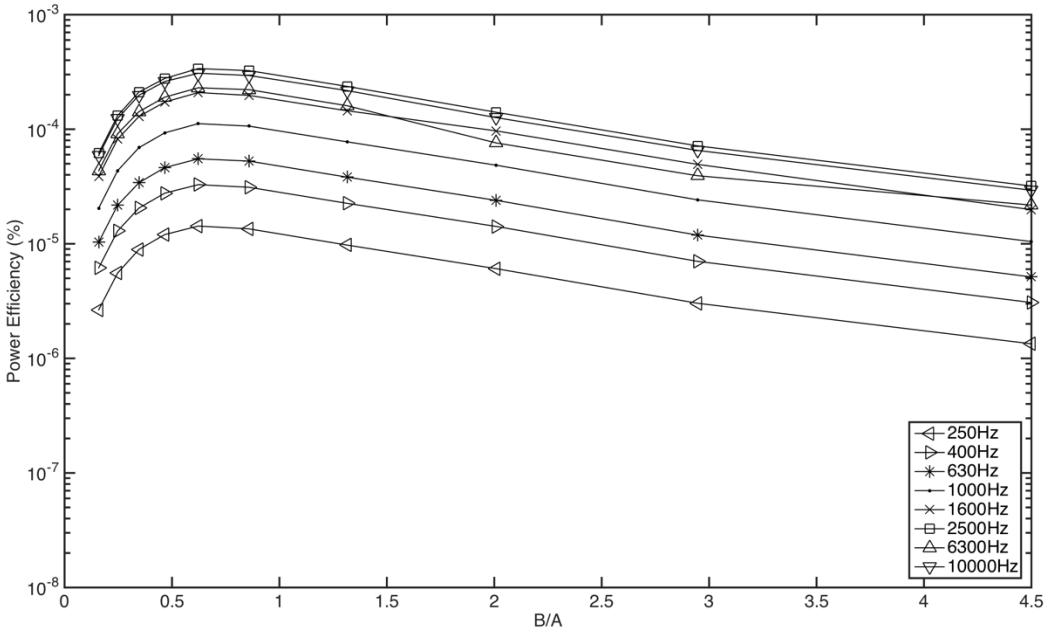

Figure 8: DCAC efficiency data for a constant power. The signal amplitude (A) and amount of DC offset (B) were both varied to get different values of B/A while keeping the total power constant at 72 W_{rms}. Efficiency was computed using Eqn. (7). Here an optimal ratio of B/A, in terms of maximum efficiency, is shown at a value of about 0.62.

Figure 7 illustrates a diminishing return on increasing the amount of DC offset (*B*). Once the ratio of *B*/*A* reaches 0.75, the increase in efficiency for the added power is marginal. Based on Figure 8, for a constant input power, a *B*/*A* ratio of 0.62 is the most optimal ratio for efficiency. The efficiency for this ratio varies from 1.69 E-6 to 308 E-6 percent between 100 Hz and 10 kHz with 72 W_{rms} total input power.

Upon exploring Figure 7 and Figure 8, a more distinct comparison between the effects of varying *B* vs *A* was desired. To achieve this, a single 1 kHz sine wave was input into the thermophone for two scenarios: holding *A* constant while changing *B* and holding *B* constant while changing *A*. Figure 9 demonstrates that increasing *B* for a constant *A* does not increase the efficiency of the CNT thermophone. Instead, increasing *A* for a constant *B* is a more efficient way of increasing the true power efficiency. Ultimately, DCAC in application would be hindered because it requires a class A/B amplifier to satisfy the need for DC offset. Common class D pulse width modulation amplifiers do not support DC offset because the rail voltages cannot differ.

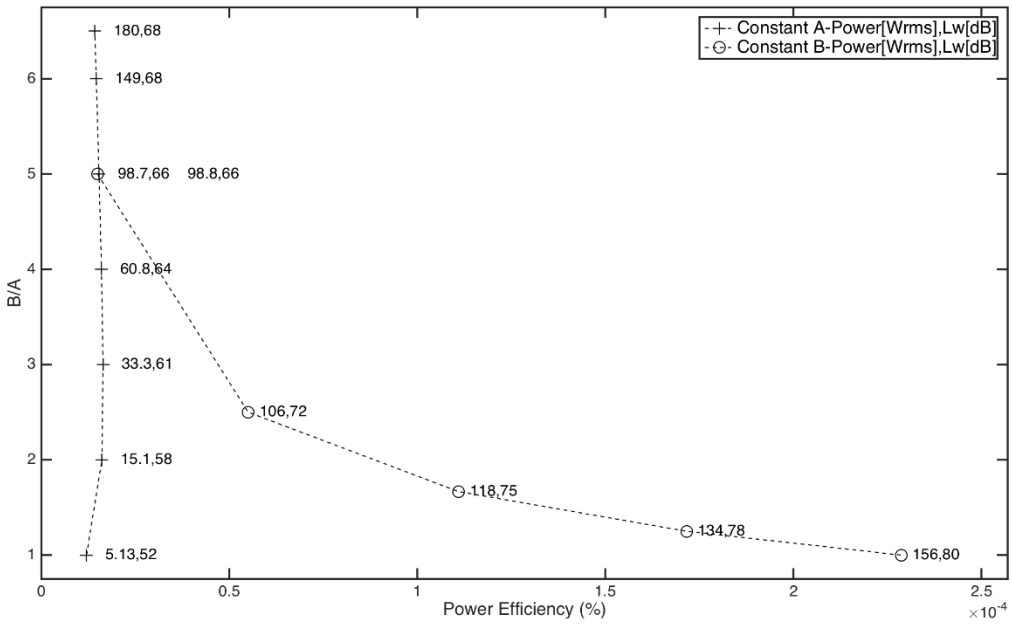

Figure 9: Data comparing the efficiency effects of holding the signal amplitude (A) constant while changing the amount of DC offset (B) vs holding B constant and changing A. The first value for each data point is the amount of power into the CNT

thermophone and the second value is the sound power (Lw) output in the 1 kHz band. Efficiency was computed using Eqn. (7). All data points were obtained using a 1 kHz sine wave.

For the AMAC technique, Figure 10 demonstrates the frequency domain acoustic output of the CNT thermophone with the frequency axis normalized by the modulation frequency. The modulated signal and its second harmonic are shown at values of F/F_m equal to 1 and 2, respectively. The carrier frequency in this example is 15 times higher than the modulation frequency. The carrier frequency is doubled and is seen at a normalized frequency of 30 with four dominant side lobes. The fundamental at $F/F_m = 15$ and fourth harmonic at $F/F_m = 60$ are not predicted by theory, but are assumed to be artifacts of imperfect signal recreation.

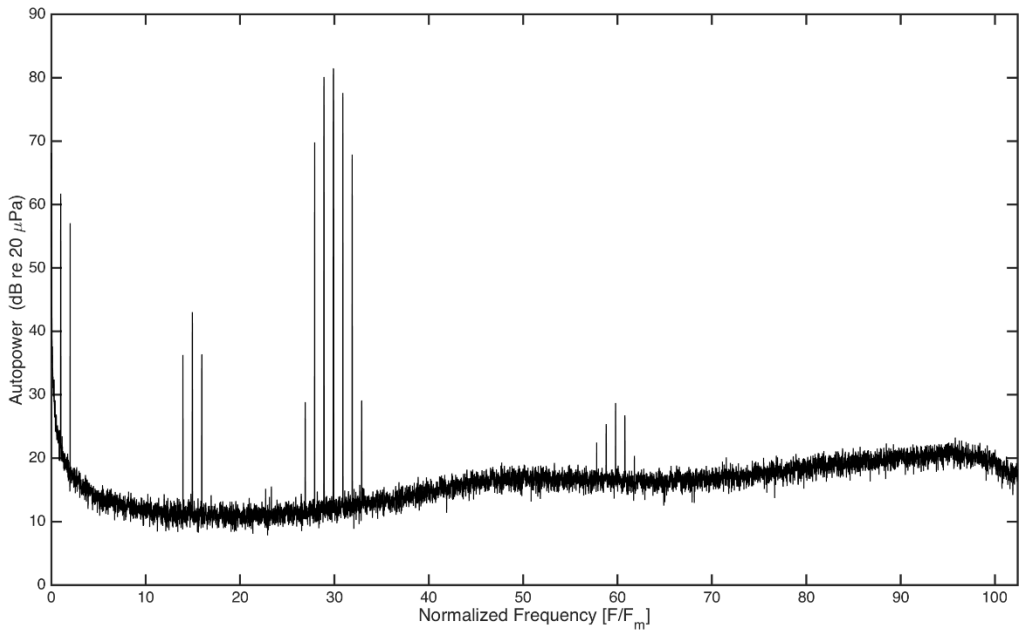

Figure 10: An example of the acoustic response of a CNT thermophone normalized to the modulation frequency. In this example, the carrier frequency is 15 times larger than the modulation frequency.

Figure 11 shows the AMAC efficiency of a CNT thermophone varies from 1.24 E-6 to 228 E-6 percent with 72 W_{rms} input power. It was found that varying the carrier frequency had no effect on the efficiency. Practically, amplitude modulation is difficult to use, because it requires an amplifier with high enough frequency response to power the carrier frequency. The human hearing range

extends to 20 kHz, meaning the AMAC carrier frequency should be greater than 20 kHz to be out of the range of hearing. Many common class D amplifiers limit their output frequency to 20 kHz, which means AMAC's utility is limited in the current market.

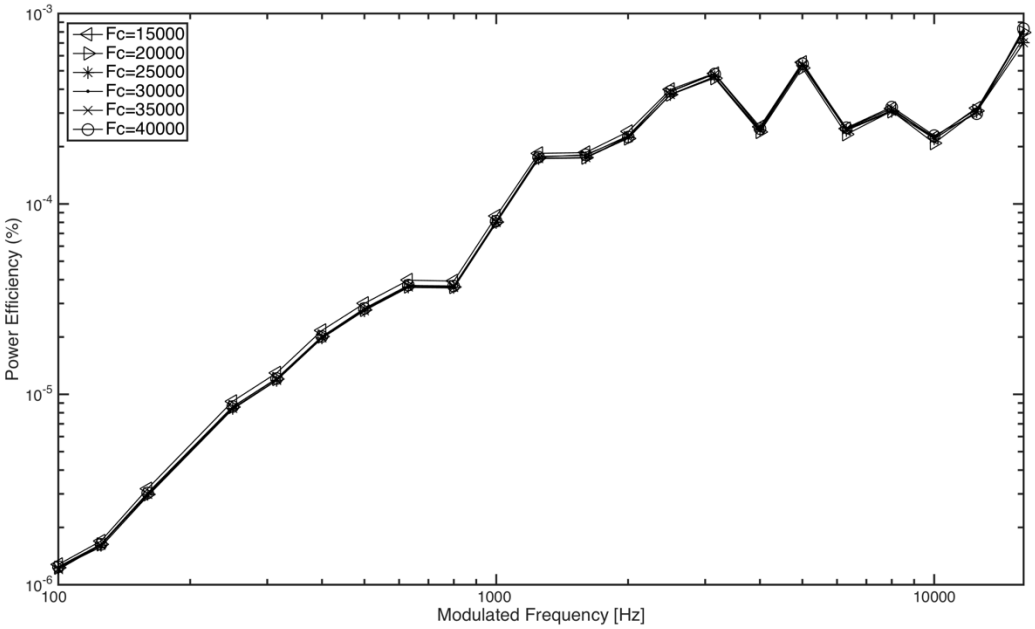

Figure 11: AMAC efficiency data. A modulated signal (F_m) was varied with carrier frequency (F_c). The modulation index for all tests was 1 and had a total input power of 72 W_{rms}. Efficiency was calculated with Eqn. (8) and was not affected by varying the carrier frequency (F_c).

Figure 12 illustrates the effects of modulation depth. The optimal efficiency is found at an amplitude modulation ratio of 1.5; however, THD effects also need to be taken into account.

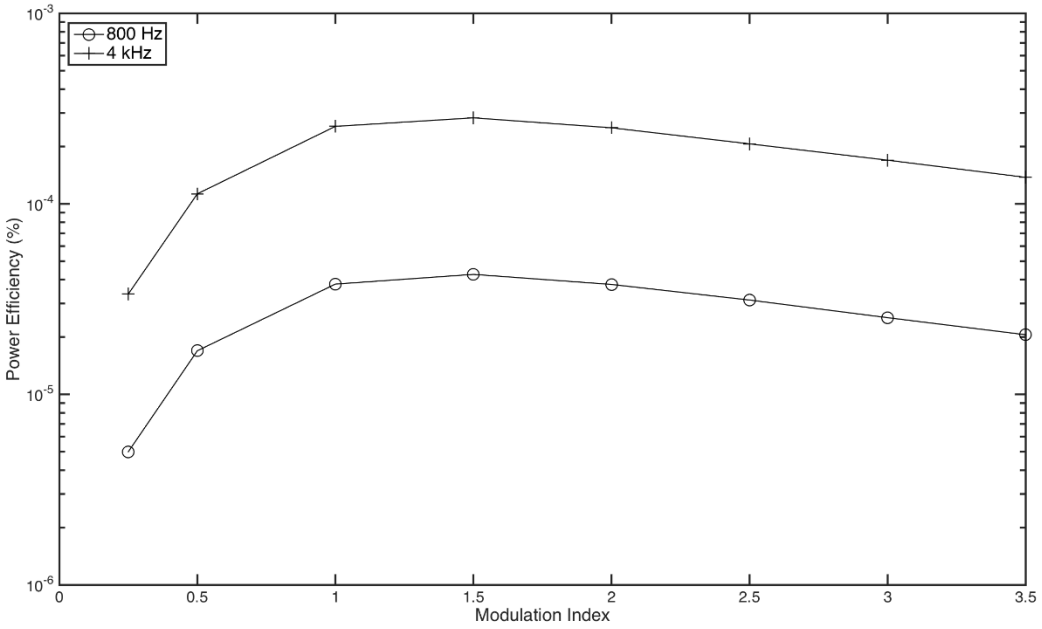

Figure 12: Experimental data illustrating the effects of varying modulation index. 72 W_{rms} total input power was used and efficiency was calculated with Eqn. (8).

Figure 13 shows the efficiency of FCAC and TCAC compared to the second harmonic AC efficiency. This shows that the FCAC and TCAC processing methods produced an efficiency of 1.01 E-6 to 1083 E-6 percent and 1.26 E-6 to 388 E-6 percent with 72 W_{rms} input power, respectively. The FCAC appears to be artificially high for frequencies above 1 kHz. The maximum efficiency should be the second harmonic AC efficiency because all of electrical energy goes into the second harmonic. For FCAC, there is some energy dispersed during the decimation process and therefore it is expected that its efficiency would be slightly less than the AC second harmonic efficiency. Regardless, the FCAC and TCAC methods are not orders of magnitude more efficient than the other signal processing techniques. Their main benefit is that with these pre-processing techniques a standard off-the-shelf amplifier can be used to power CNT thermophones.

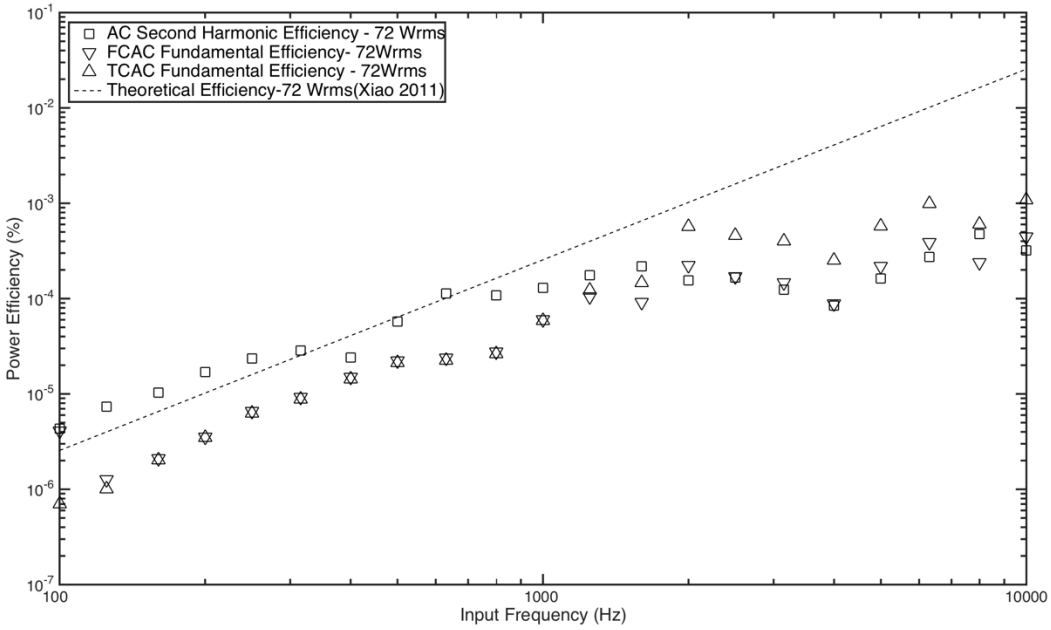

Figure 13: Experimental data comparing second harmonic AC efficiency to fundamental FCAC and TCAC efficiency. 72 w_{rms} total input power was used and efficiency for AC was calculated using Eqn. (6) and efficiency for FCAC and TCAC was calculated using Eqn (9).

Figure 14 and Figure 15 compare the THD for the DCAC method. They demonstrate that increasing *B*/*A* decreased THD, but there was a diminishing return; the more *B*/*A* increased the less reduction in THD was observed. Since THD does not have a threshold level where content becomes intelligible, the value of *B*/*A* required for an acceptable level of THD will be subjective. Based on optimal efficiency and Eqn. (4), a *B*/*A* level of 0.62 produces THD in the 43-93% range. A *B*/*A* ratio of 0.62 created subjectively intelligible content for the author, but the THD was roughly 65 times higher than a standard moving coil loudspeaker (Table 3). It should be noted that intelligibility and high fidelity are not the same thing.

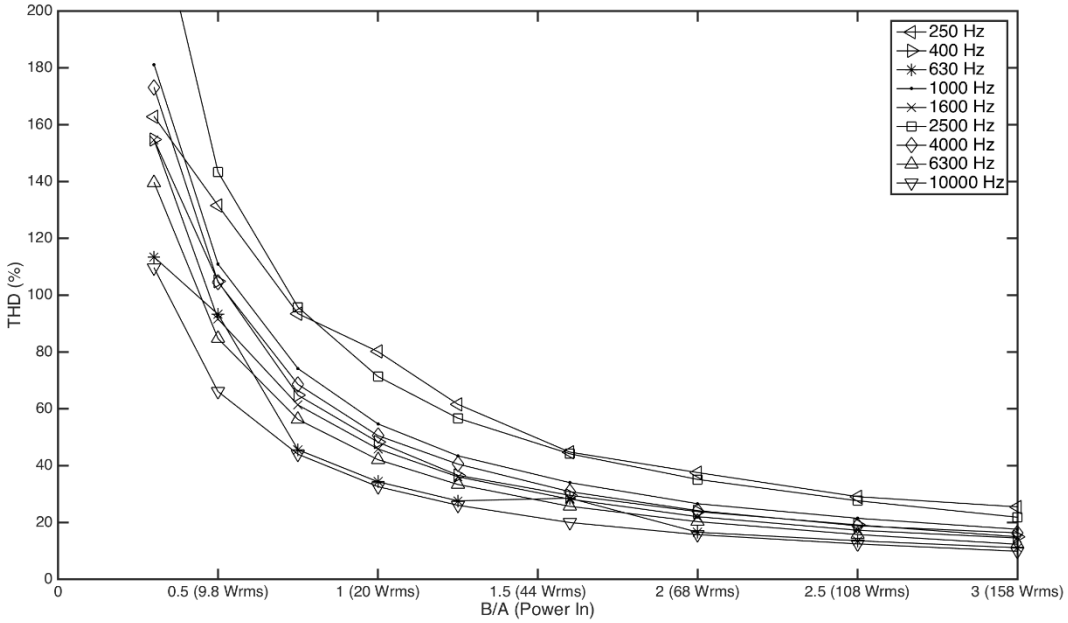

Figure 14: Data comparing THD for different frequencies and ratios of B/A for different input power levels. A was held constant and B was increased. THD was computed with Eqn. (4).

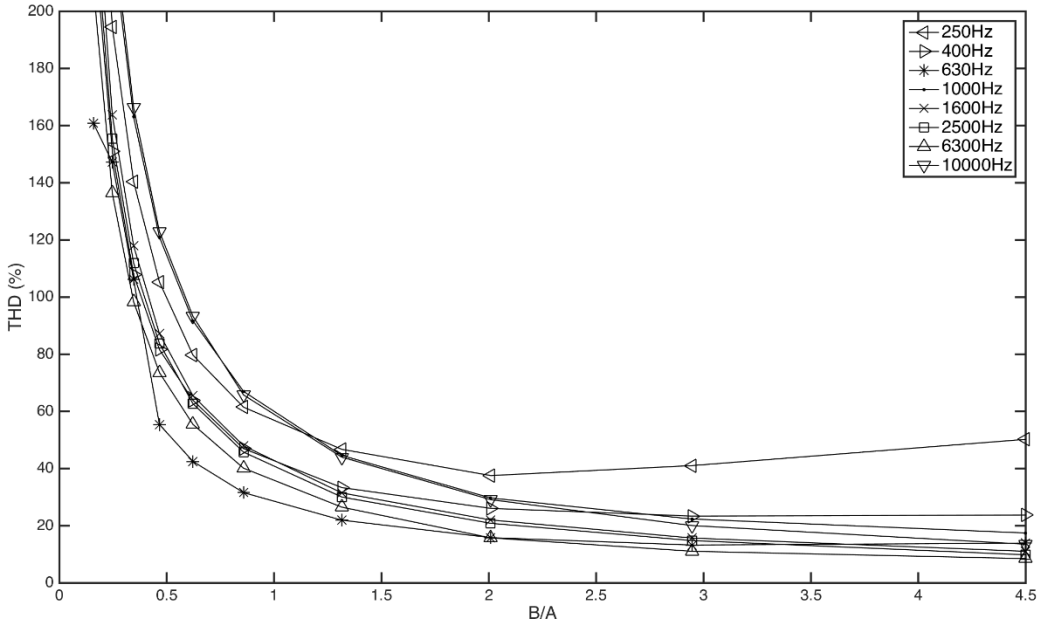

Figure 15: Data comparing THD for varying frequencies and ratios of B/A. In this case B and A were manipulated to get a constant power of 72 W_{rms} input to the CNT thermophone for each case. THD was computed with Eqn. (4).

Figure 16 demonstrates that THD for AMAC varies from 22-95%. For certain higher frequencies where the carrier was a harmonic of the modulated frequency, THD was significantly higher, but this should not cause any practical issues as long as the carrier is above 20 kHz. From a modulation index perspective, THD increased rapidly as modulation index was increased (Figure 17). Therefore, while the optimal modulation index for efficiency is 1.5, the THD increased significantly from 1 to 1.5. A modulation index of 1.0 is the best compromise between efficiency and THD.

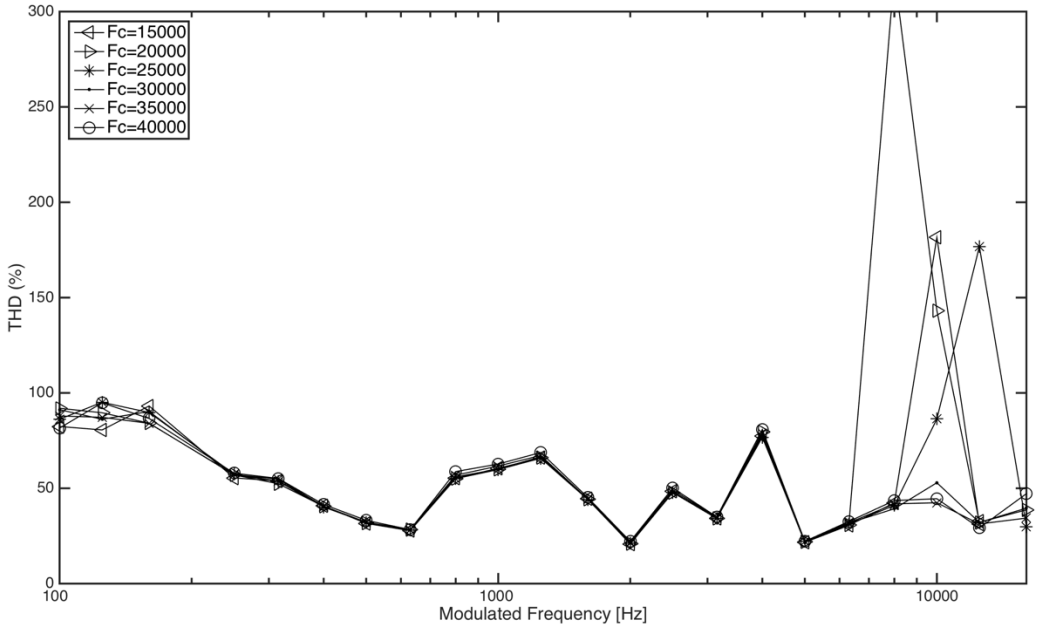

Figure 16: THD data for AMAC. The lack of correlation in the high frequency region is a result of the carrier frequency being at a harmonic of the fundamental. Therefore, the THD was artificially increased by the carrier. THD was computed with Eqn. (4).

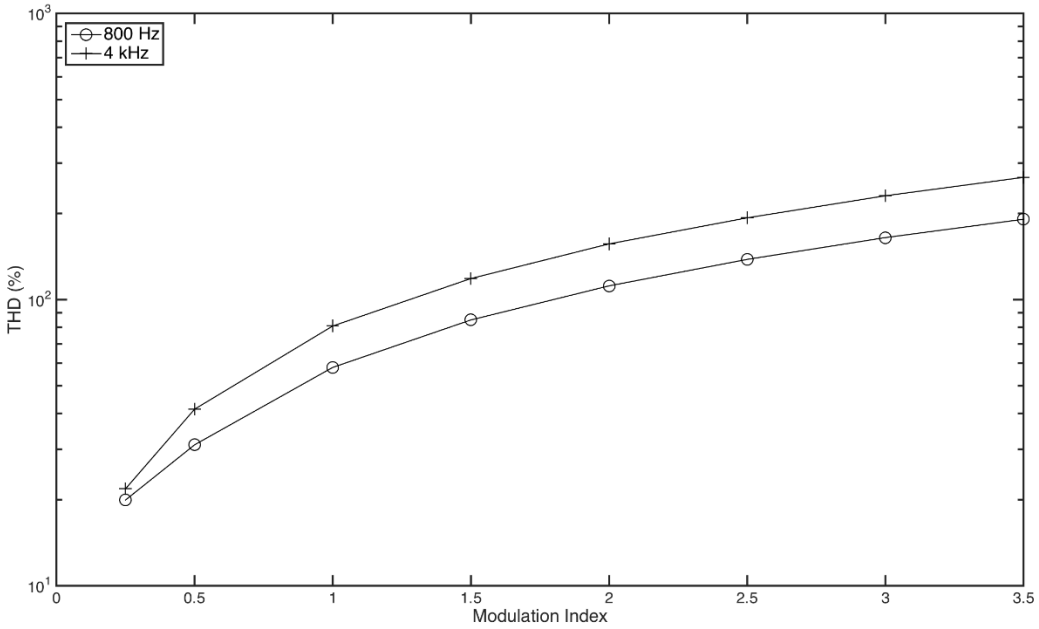

Figure 17: Data showing the effects on THD for varying modulation index. THD was computed with Eqn. (4).

Figure 18 demonstrates that the THD for FCAC and TCAC vary from 0.68-59% and 1.7-11%, respectively. This is better than the DCAC and AMAC processing techniques, but it should be noted that these are for single frequencies. When the FCAC and TCAC algorithms are optimized for single frequencies they can create almost perfect half frequency content. When processing complex signals these methods are inhibited. For example, subjectively using speech and music the FCAC and TCAC produced significantly less intelligible reproduction, in the author's opinion, compared to DCAC and AMAC. Therefore, THD is not the best sound quality metric to compare DCAC, AMAC, FCAC, and TCAC.

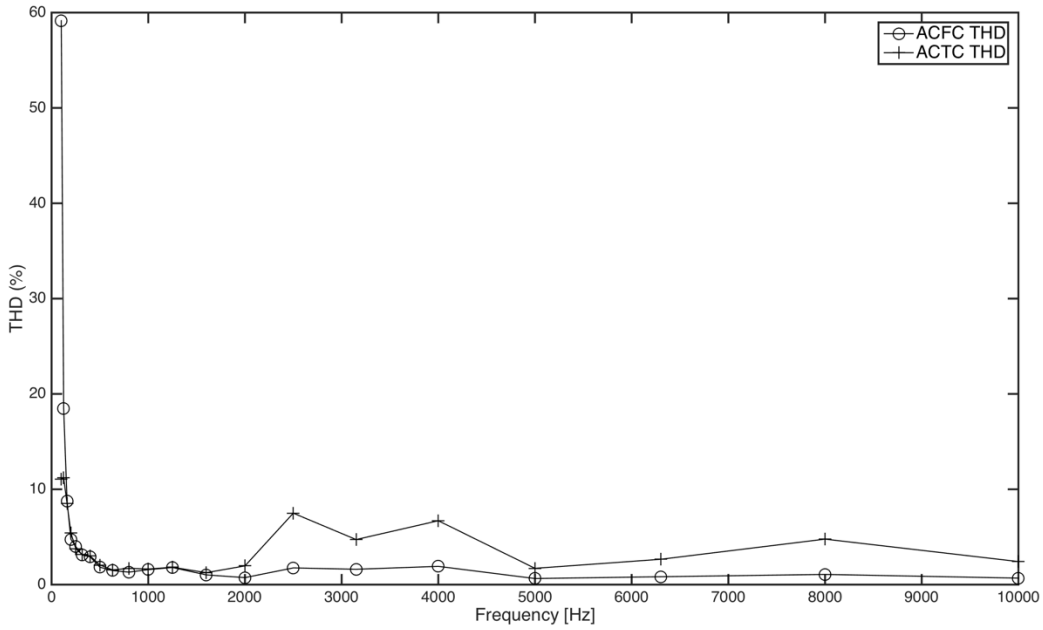

Figure 18: Data showing THD for FCAC and TCAC. THD was computed using Eqn. (4).

A summary comparison of AC, DCAC, AMAC, FCAC, and TCAC is shown in Table 4.

Table 4: Summary of experimental data for AC, DCAC, and AMAC signal processing techniques. The total input power for all tests was 72 W_{rms} with frequency ranges of 100 Hz to 10 kHz. Note that the efficiency for the AC case is the second harmonic efficiency.

	Efficiency (μ%)	THD (%)
AC	4.3 - 319	$\approx \infty$
DCAC (B/A=0.62)	1.69 - 308	43 - 93
AMAC	1.24 - 228	22 - 95
FCAC	1.01 - 1083	0.68 - 59
TCAC	1.26 - 388	1.7 - 11

4 Conclusions

The fundamental true efficiency of an AC signal is approximately zero due to the non-linearity of CNT thermophones. The second harmonic efficiency of a CNT thermophone is 4.3 E-6 to 319 E-6 percent for 72 W_{rms} input. Experimentally, the efficiency is directly proportional to the input power, which supports the theoretical model created by Xiao et al.[14] Additionally, the Xiao et al. model matched experimental efficiency data for frequencies below 1,600 Hz, where the sound source radiates as a monopole. For DCAC, the optimal efficiency ratio of DC offset to signal amplitude was found to be 0.62. The fundamental true efficiency with that ratio is 1.69 E-6 to 308 E-6 percent for 72 W_{rms} input. This ratio had a THD varying from 43-93%. In terms of AMAC, the fundamental true efficiency is 1.24 E-6 to 228 E-6 percent. Varying the carrier frequency had no effect on efficiency. Additionally, the optimal modulation index in terms of efficiency is 1.5, but when considering THD an index of 1.0 gives the best efficiency for the least amount of THD of 22-95%. Therefore, AMAC has better THD than DCAC with slightly lower efficiencies. Ultimately, DCAC and AMAC are less efficient than AC, but the overall efficiency loss is small, so these methods may prove to be sufficient. Their main limitation is the requirement of special amplifiers. DCAC required a class A/B amplifier that can apply a DC offset, and AMAC requires an amplifier that can output frequencies as high as the sum of the carrier and modulated frequencies. FCAC and TCAC allow for no special amplification and would allow for easier market entrance. Their efficiencies were 1.01 E-6 to 1083 E-6 percent and 1.26 E-6 to 388 E-6 percent with 72 W_{rms} input power, respectively. They had THD of 0.68-59% and 1.7-11%, respectively. Ultimately, THD was found to be a poor sound quality metric to compare DCAC, AMAC, FCAC, & TCAC for complex signals.

5 Future work

Based on the work completed, signal processing as a means to increase the efficiency of CNT thermophones is limited. If CNT loudspeakers are truly going to enter the market in more than an extremely niche way, their efficiency and ruggedness will need to be improved. As the pervious work shows, efficiency and sound quality are often competing factors. Therefore, it will be important to understand how to quantify sound quality for these devices as their efficiency and ruggedness are further optimized.

5.1 Technology Needs

The current technology needs for CNT loudspeakers are efficiency and ruggedness optimization through the drive signal processing, sound quality investigation, heat recycling, modeling, enclosure designs, diaphragm material, and surrogate material development (Figure 19).

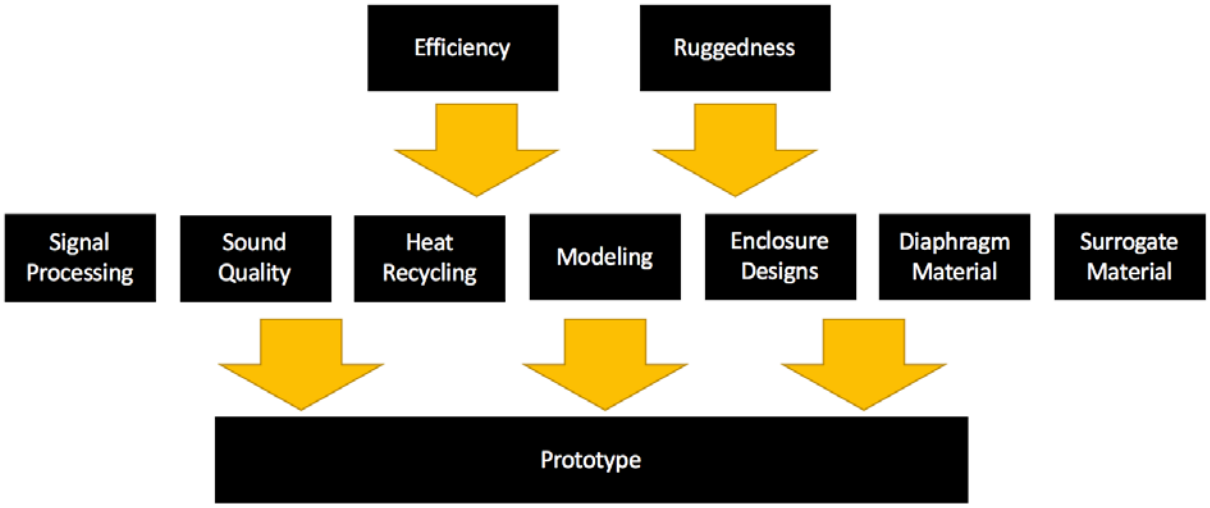

Figure 19: Graphic outlining the overall view of future work needed on CNT loudspeakers.

The signal processing work is complete with respect to efficiency, although new methods developed in the future could be easily explored using the testing methodology introduced here. The work presented in this report and work by Barnard et al.[10,11] are the only published works

exploring sound quality with respect to CNT thermophones. Moving forward, a detailed understanding of CNT loudspeakers with respect to their sound quality would give the acoustic community insight on their viability in many more applications as well as an ability to validate true gains in efficiency. For example, if a researcher developed a method to significantly improve the efficiency of CNT loudspeakers, but drastically decreased their sound quality this development would be inferior to a method that did not decrease sound quality. The main issue today is that the best method to quantify sound quality with respect to CNT loudspeakers is unknown.

Heat recycling should be explored as a way to increase system efficiency. The idea is to use a thermoelectric generator to convert some of the heat back into electricity. The main challenge of this work will be figuring out how to get the power created back to the rails of the amplifier. While current thermoelectric generators (TEGs) operate around 5% efficient[23], they have rarely been used for temperature differentials as high as CNTs, 2000 Celsius in Argon[24]. This should lead to higher TEG efficiency and bring that benefit to the loudspeaker. Novel TEG designs are currently under development by many researchers, hopefully resulting in higher efficiency devices that can be used for enclosed CNT thermophones.

Modeling of the CNT thermophone would allow ease in development of these devices. A validated model would show true understanding of the physical phenomena as well as allow for extrapolation of current ideas with relatively simple effort. The multi-physics model would be complex in its need to couple the electrical, thermal, and acoustic domains. This is the current work of graduate student Mahsa Asgarisabet at Michigan Technological University.

Enclosure design optimization is also needed. These enclosures will need to be acoustically optimized. For example, it has been proven that enclosing the thermophone in inert gas increases

the efficiency[6,14]. The initial inert gas work has been expanded to explore the effects of CNT enclosures with the inert gas, film separation and heat sinks to allow the system to be more rugged[24]. The enclosure will have to be designed for broadband excitation and not a single resonance[25]. Additionally, exploration for the best surrogate/backing material to place the CNT on is needed. Having this surrogate material will provide a 6 dB increase in SPL, but requires optimization of the gap distance[25]. Additionally, a diaphragm material will have to be selected. The material will have to be optimized to be able to couple the inside acoustic wave to the outside air while being able to handle the high heat. Thermoacoustic generation in the future may also include looking outside of carbon nanotube thin films. Sound has been created successfully with graphene sheets[26-28] and CNT foams[29].

5.2 Proposed work.

Goal: Complete a thorough investigation of objective and subjective sound quality with respect to input signal processing of drive signals for carbon nanotube thin-film loudspeakers.

As of today the work presented in this report along with work done by Barnard et al.[10,11] are the only published works discussing or quantifying sound quality for CNT loudspeakers. These works only use single tone THD and demonstrates the need for a way to compare complex signals. This work specifically demonstrates the direct link between efficiency and sound quality. Today there is a need to understand the true sound quality differences between standard moving coil loudspeakers and CNT loudspeakers for potential use in many applications. In the future as developments in efficiency are made a scientific way to compare those developments with regards to sound quality will be needed. Therefore, this proposed work revolves around five key milestones:

1. Throughout the entire process, continue to evaluate emerging signal processing techniques for sound quality and efficiency.
2. Explore sound quality metrics and compare them to standard speakers.

3. Conduct jury studies to get subjective comparisons between CNT speakers and standard speakers. Jury studies will focus on word intelligibility using phonetically balanced words, the modified rhyme test, and/or other techniques. In addition, music comparison will be rated using subjective jury analysis.
4. Correlate sound quality metrics to jury results and develop design criterion for thermophone sound quality.
5. Determine which type of signal processing results in the best compromise between efficiency and sound quality.

It will be important for this work to remain flexible and allow for new processing techniques to be incorporated into the project as they are developed. For the second milestone, current sound quality metrics used in the loudspeaker industry as well as other industries will be investigated. From these a list of objective metrics will be experimentally tested on a standard loudspeaker and a CNT loudspeaker using multiple signal processing techniques. This objective data will be the first step in the comparison between standard and CNT loudspeakers.

For the third milestone, a jury study will be undertaken to subjectively compare standard moving coil loudspeakers to CNT loudspeakers. This study will focus on word intelligibility as well as music comparison. Word intelligibility will be explored with phonetically balanced words and the modified rhyme test. Other methods will also be explored as a better understanding of the test becomes known. It will be important to understand the word intelligibility between standard and CNT loudspeakers for any public address (PA) system setup or applications where speech will be projected through the loudspeaker. Additionally, a music comparison between standard and CNT loudspeakers will allow for a more defined application space for CNT loudspeakers. For example, if their sound quality is good enough to replace loudspeakers in the automotive industry then that industry can reap the weight savings.

As of today only single tone THD is understood. The correlation of an in depth objective and subjective comparison of standard and CNT loudspeakers will provide the acoustic community with important information needed to understand where CNT loudspeakers can and cannot be used

based on their specific design criteria. With these objective and subjective studies an important understanding of the factors that play a role in CNT loudspeaker sound quality will also be determined. These will be especially important to the community as they work to use this new tool in their application space.

Finally, from all of this work a determination of which input processing techniques provide the best compromise between efficiency and sound quality can be concluded. While this may not be relative to the automobile industry, for example, where excess power is easier to come by, this will be extremely important in applications where efficiency is key. For example, if CNT loudspeakers were ever used in a mobile phone application, the ideal compromise between efficiency and sound quality will be desired. Additionally, in large hail and warning device applications for the military where weight, sound quality, and efficiency are key, knowing the ideal processing technique will be important. Throughout the continued work on this project, the affects of sound quality on all other aspects of thermophone development (e.g. enclosure design, surrogate materials, etc…) will be noted. Ultimately, a significantly better understanding of CNT loudspeaker sound quality will be obtained through this project.

5.2.1 Milestones

The following outlines the milestones towards the completion of the doctoral degree.

Milestone 1: Determination of drive signal processing techniques to use in future work

-Optimize FCAC & TCAC for complex signals

-Investigate additional signal processing techniques

-E.g. how does YouTube frequency shift its audio when increasing video speed.

-If new techniques are found, obtain experimental efficiency/THD data on them. Then write paper with data from the new techniques, FCAC, & TCAC. If no new methods are found at least write a conference paper on FCAC TCAC efficiency/THD data.

Milestone 2: Quantify sound quality for CNT thermophones based on current metrics

-Research a large amount of current metrics (e.g. STIPA)

-Experimentally quantify sound quality with current metrics

-Develop new metric if needed

-Write paper on the data obtained

Milestone 3: Completion of a jury study comparing CNT to standard moving coil loudspeakers based on the current list of drive signal processing techniques

-Development of the test

-Phonetically balanced words

-Modified rhyme test

-Others tests found relevant

-Music comparison

-IRB approval

-Development of automated system to conduct study

-Write paper on the results

Milestone 4/5: Correlation of sound quality metric results to jury study results

-Develop criteria for thermophone sound quality

-Determine which type of drive signal processing results in the best compromised between efficiency and sound quality.

-Write paper on correlation, criteria, and best drive signal processing technique.

Summer 2019: Defend

References

[1]T. Bouman, M. Asgarisabet & A. Barnard, “Experimental quantification of the true efficiency of carbon nanotube thin-film thermophones,” *J. Acoust. Soc.Am.* 139.3, 1353-1363 (2016). http://dx.doi.org/10.1121/1.4944688

[2]F. Braun, “Notiz über Thermophonie” (“Note on thermophonie”), *Ann. Der Physik* 65, 358–360 (1898). http://dx.doi.org/10.1002/andp.18983010609

[3]H. Arnold & I. Crandall, “The thermophone as a precision source of sound,” *Phys.* Rev. 10, 22–38 (1917). http://dx.doi.org/10.1103/PhysRev.10.22

[4]S. Iijima, "Helical microtubules of graphitic carbon," *Nature* 354.6348, 56-58 (1991). http://dx.doi.org/10.1038/354056a0

[5]X. Yu, R. Rajamani, K. Stelson & T. Cui, “Carbon nanotube-based transparent thin film acoustic actuators and sensors,” *Sensors and Actuators A: Physical*, 2006 *132*(2), 626-631, pp http://dx.doi.org/10.1016/j.sna.2006.02.045

[6]A. Aliev, Y. Gartstein & R. Baughman, "Increasing 405 the efficiency of thermoacoustic carbon nanotube sound projectors," *Nanotechnology* 24(23), 235501 (2013). http://dx.doi.org/10.1088/0957-4484/24/23/235501

[7]A. Aliev, M. Lima, S. Fang & R. Baughman, "Underwater sound generation using carbon nanotube projectors," *Nano Lett.*, 2010, 10 (7), pp 2374–2380. http://dx.doi.org/10.1021/nl100235n.

[8]A. Barnard, D. Jenkins, T. Brungart, T. McDevitt & B. Kline, “Feasibility of a high-powered carbon nanotube thin-film loudspeaker,” *J. Acoust. Soc.Am.* 134, EL276–EL281 (2013). http://dx.doi.org/10.1121/1.4817261

[9]A. Barnard, T. Brungart, T. McDevitt & D. Jenkins “Background and development of a high powered carbon nanotube thin-film loudspeaker,” *Proceedings of Inter-Noise, New York, USA, 2012.*

[10]A. Barnard, T. Brungart, T. McDevitt, A. Aliev, D. Jenkins, B. Kline & R. Baughman, "Advancements toward a high-power, carbon nanotube, thin-film loudspeaker," *Noise Control Engineering Journal* 62(5), 360-367 (2014). http://dx.doi.org/10.3397/1/376235

[11]A. Barnard, T. Brungart, T. McDevitt, D. Jenkins & B. Kline, “Advancements toward a high powered carbon nanotube thin-film loudspeaker,” *Proceedings of Noise-Con*, Denver, USA, 2013.

[12]L. Xiao, Z. Chen, C. Feng, L. Liu, Z. Bai, Y. Wang, L. Qian, Y. Zhang, Q. Li, K. Jiang & S. Fan, “Flexible, stretchable, transparent carbon nanotube thin-film loudspeakers,” *Nano Lett.* 8(12), 4539–4545 (2008). http://dx.doi.org/10.1021/nl802750z

[13]S. Asadzadeh, A. Moosavi, C. Huynh & O. Saleki, “Thermo acoustic study of carbon nanotubes in near and far field: Theory, simulation, and experiment,” *Journal of Applied Physics*, *117*(9), 095101 (2015). http://dx.doi.org/10.1063/1.4914049

[14]L. Xiao, P. Liu, L. Liu, Q. Li, Z. Feng, S. Fan & K. Jiang, “High frequency response of carbon nanotube thin-film speaker in gases,” *J. Appl. Phys.* 110(8), 084311 (2011). http://dx.doi.org/10.1063/1.3651374

[15]B. Mason, S. Chang, J. Chen, S. Cronin & A. Bushmaker, “Thermoacoustic transduction in individual suspended carbon nanotubes,” *ACS nano* (2015). http://dx.doi.org/10.1021/acsnano.5b01119

[16]M. Kozlov, C. Haines, J. Oh, M. Lima & S. Fang, "Sound of carbon nanotube assemblies," *J. Appl. Phys.* 106(12), 124311 (2009). http://dx.doi.org/10.1063/1.3272691

[17]B. Moore, C. Brian, B. Glasberg & M. Stone. "Optimization of a slow-acting automatic gain control system for use in hearing aids." *British journal of audiology* 25.3 (1991): 171-182. http://dx.doi.org/10.3109/03005369109079851

[18]J. Alexander, J. Kopun, & P. Stelmachowicz, "Effects of frequency compression and frequency transposition on fricative and affricate perception in listeners with normal hearing and mild to moderate hearing loss," *Ear and hearing* 35.5 (2013): 519-532.

[19]J. Pöhls, M. Johnson, M. White, R. Malik, B. Ruff, C. Jayasinghe, M. Schulz & V. Shanov, “Physical properties of carbon nanotube sheets drawn from nanotube arrays,” *Carbon*, *50*(11), 4175-4183 (2012). http://dx.doi.org/10.1016/j.carbon.2012.04.067

[20]M. Jakubinek, M. White, G. Li, C. Jayasinghe, W. Cho, M. Schulz & V. Shanov, “Thermal and electrical conductivity of tall, vertically aligned carbon nanotube arrays,” *Carbon*, *48*(13), 7-3952 (2010). http://dx.doi.org/10.1016/j.carbon.2010.06.063

[21]ANSI S12.54, “Acoustics - Determination of sound power levels and sound power levels of noisesources using sound pressure - Engineering methods for an essentially free field over a reflectingplane,” *American National Standards Institute*, New York (2011).

[22]S. Garrett, “Two-Way Loudspeaker Enclosure Assembly and Testing as A Freshmen Seminar,” *Proceedings of Congress On Sound & Vibration 17*, Cairo, Egypt, 2010.

[23]B. Riffat, & X. Ma, “Thermoelectrics: a review of present and potential applications,” *Applied Thermal Engineering*, 23(8), 913-935. (2003). http://dx.doi.org/10.1016/S1359-4311(03)00012-7

[24]A. Aliev, N. Mayo, R. Baughman, D. Avirovik, S. Priya, M. Zarnestske & J. Blottman, "Thermal management of thermoacoustic sound projectors using a free-standing carbon nanotube

aerogel sheet as a heat source," *Nanotechnology* 25.40 (2014): 405704. http://dx.doi.org/10.1088/0957-4484/25/40/405704

[25]L. Tong, C. Lim & Y. Li, "Gas-filled encapsulated thermal-acoustic transducer," *Journal of Vibration and Acoustics* 135.5 (2013): 051033. http://dx.doi.org/10.1115/1.4024765

[26]C. Kim, S. Hong, J. Lee, D. Kang, B. Cho & J. Choi, "Free-Standing Graphene Thermophone on a Polymer-Mesh Substrate," *Small* 12.2 (2016): 185-189. http://dx.doi.org/10.1002/smll.201501673

[27]H. Tian, T. Ren, D. Xie, Y. Wang, C. Zhou, T. Feng, D. Fu, Y. Yang, P. Peng, L. Wang & L. Liu, "Graphene-on-paper sound source devices," *ACS nano* 5.6 (2011): 4878-4885. http://dx.doi.org/10.1021/nn2009535

[28]H. Tian, D. Xie, Y. Yang, T. Ren, Y. Wang, C. Zhou, P. Peng, L. Wang & L. Liu, "Single-layer graphene sound-emitting devices: experiments and modeling," *Nanoscale* 4.7 (2012): 2272-2277. http://dx.doi.org/10.1039/C2NR11572G

[29]A. Aliev, N. Mayo, M. Jung de Andrade, R. Robles, S. Fang, R. Baughman, M. Zhang, Y. Chen, J. Ah Lee & S. Jeong Kim, "Alternative Nanostructures for Thermophones," *ACS nano* 9.5 (2015): 4743-4756. http://dx.doi.org/10.1021/nn507117a

Appendix A: Experimental Setup

In order to measure the efficiency of the CNT thermophone, an automated test fixture was designed, fabricated, and validated. In the 6th floor anechoic chamber at Michigan Technological University there is not enough room to complete an ANSI S12.54 sound power test. This is because there is no way to create a 1 m hemisphere inside the compact space. To automate the testing and allow for the standard to be implemented, a stepper motor connected to a lazy-Susan style turn table was created. This table was used to turn the source through an arc of four microphones (Figure 2 & Figure 3). This appendix will describe how the fixture was design/fabricated, programmed, and validated.

A.1 Design/Fabrication

First, the chamber was modeled in SolidWorks to get a better idea of what was possible in the space (Figure A1). A 1 m hemisphere had to be possible while still keeping the microphones and source far enough away from the foam wedges to ensure a direct field. From there, a stepper motor controlling a lazy-Susan style turn table was decided on (Figure A2). A CNT fixture was designed and fabricated as well (Figure A3). The components used to fabricate the test and CNT fixture are shown in Table A1 & Table A2 &, respectively. Fabrication was completed in spring of 2015. Figure A4, Figure A5, Figure A6, Figure A7, & Figure A8 show the finished assembly.

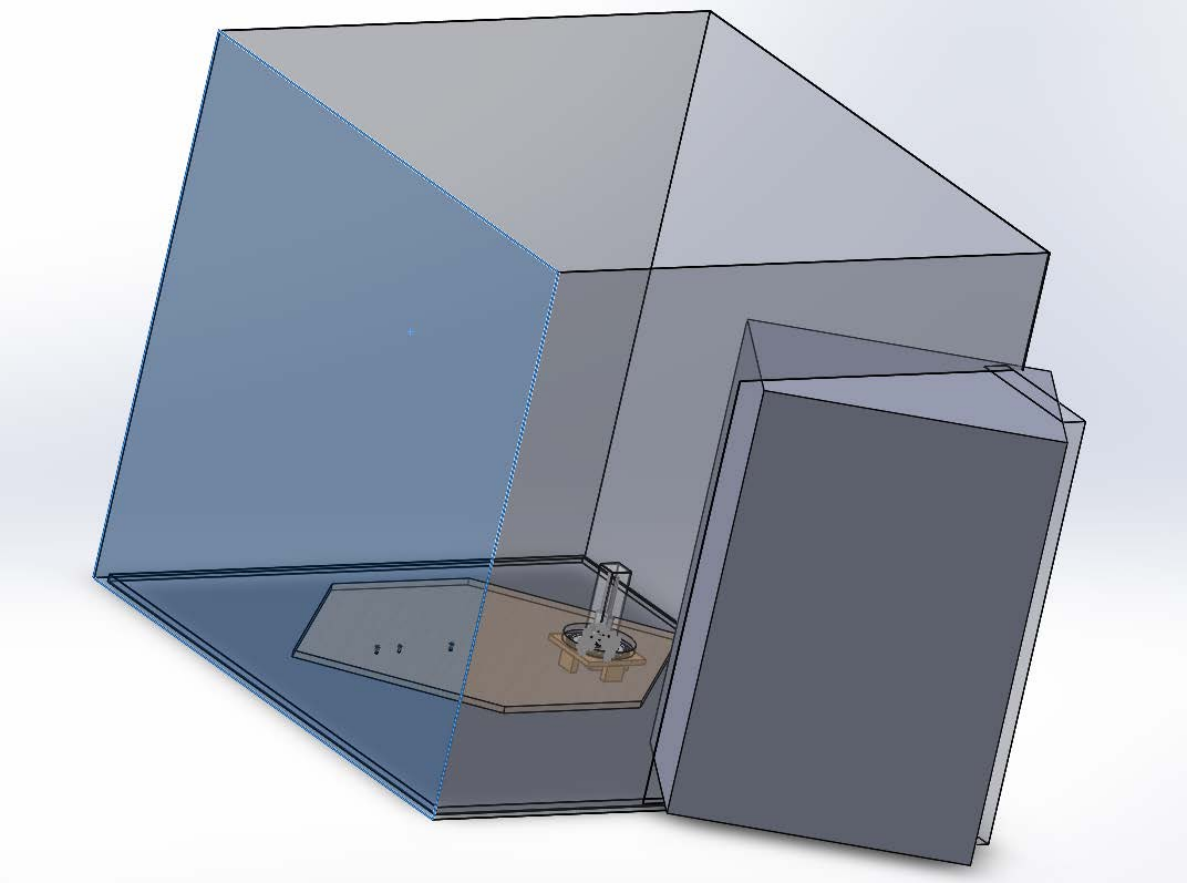

Figure A1: SolidWorks model of the sound power test fixture inside of the anechoic chamber.

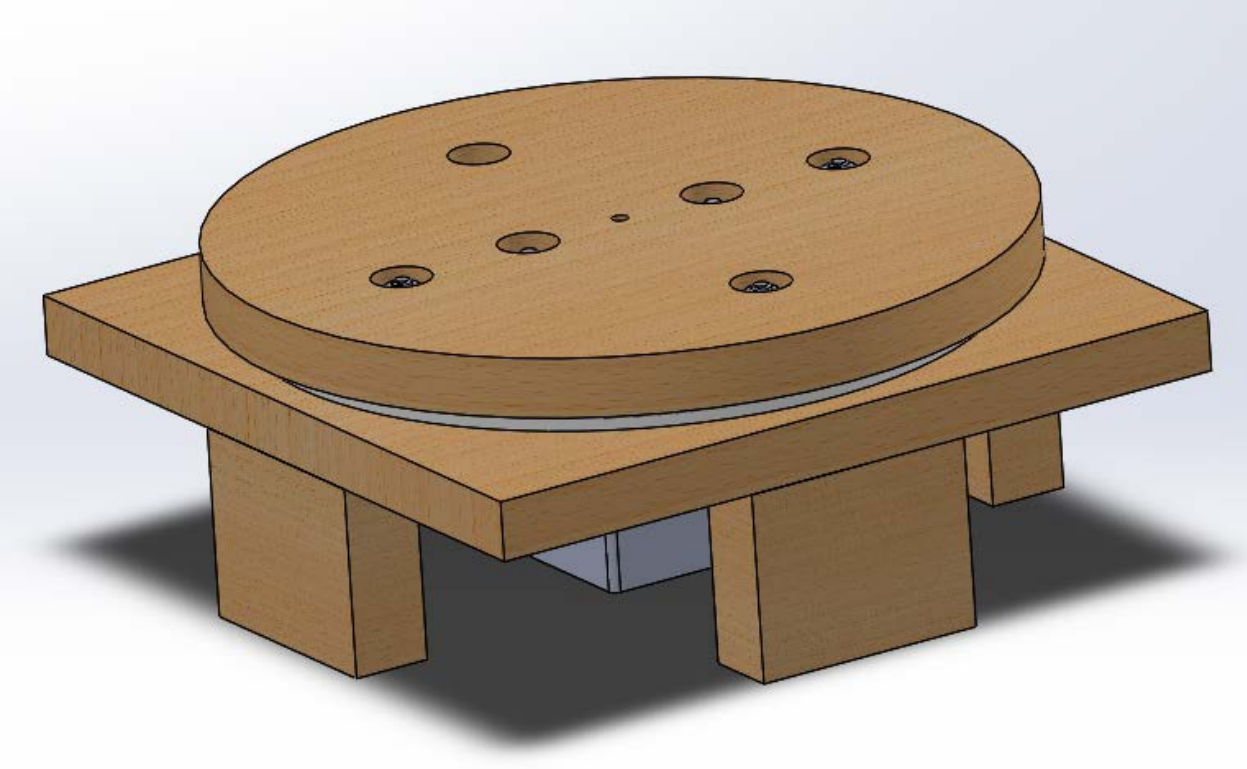

Figure A2: SolidWorks model of the lazy susan design used.

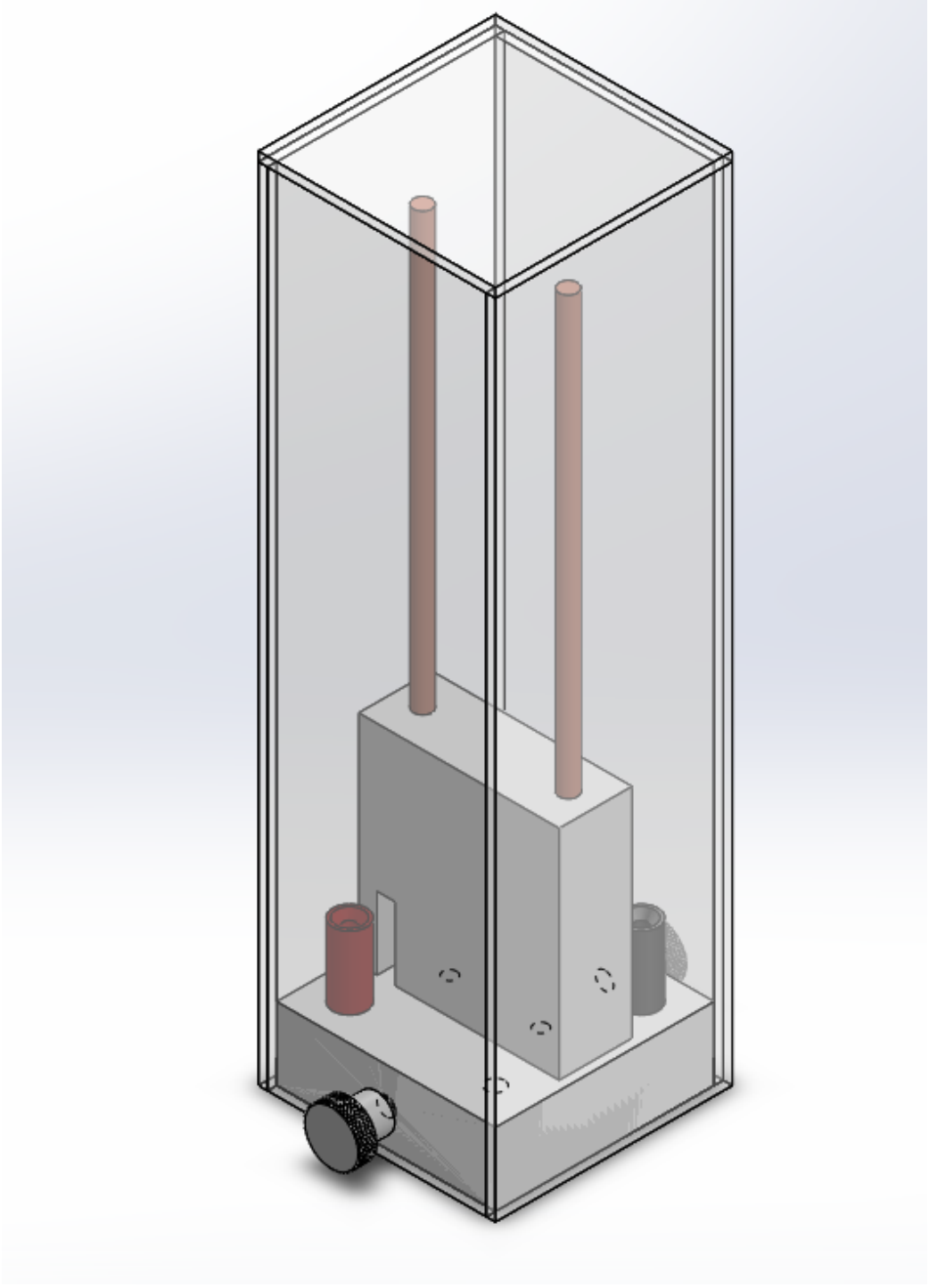

Figure A3: SolidWorks model of the CNT fixture designed and built in fall of 2014. The CNT is stretched over the two copper rods and is protected by a plexi glass enclosure.

Table A1: Sound power fixture BOM. Some items were already in stock so they did not need to be purchased.

Item	Price
4'x4'x.75" MDF base plate	$35.00
2'x4'x8	$12.00
1/4-20x.75 button head cap screws x6	$-
10-24x.75 button head cap screws x4	$-
10-32x.75 button head cap screws x4	$-
.25x.5x12" 6061	$-
1/4-20 lock washers	$-
LZSusan Bearing	$6.38
Stepper Motor	$-
Encoder	$42.00
NI 9512	$489.60
Cabling to connect stepper	$27.90
Cabling to connect encoder	$37.80
24V power supply	$20.00
NI Chassis	$-
Total=	$670.68

Table A2: CNT Fixture BOM

Item	Price	Link
Teflon 3x6"	$87.65	http://www.mcmaster.com/#8743k24/=tkbudp
10-24 flat head socket cap screws 2" long	$7.60	http://www.mcmaster.com/#91253a255/=tkbhk4
101 super conductive copper rod 2ft	$12.70	http://www.mcmaster.com/#8965k12/=tkbw0f
4"x4ftx0.125" plexiglass	$9.20	http://www.mcmaster.com/#1227t169/=tkbyzf
Hand Knobs	$8.10	http://www.mcmaster.com/#6079k13/=tkc6dq
Weld-on #3 acrylic glue	$16.74	http://www.mcmaster.com/#7528a13/=tkeund
Plastic droppers	$2.35	http://www.mcmaster.com/#7029t1/=tkeu3r
Red 5 way binding post	$3.98	http://www.parts-express.com/gold-binding-post-pair-insulated--091-1140
Black 5 way binding post	$3.98	http://www.parts-express.com/gold-binding-post-pair-insulated--091-1140
Total	$152.30	

Figure A4: Final sound power fixture being used to measure the sound power of a blender for MEEM 4704 lab.

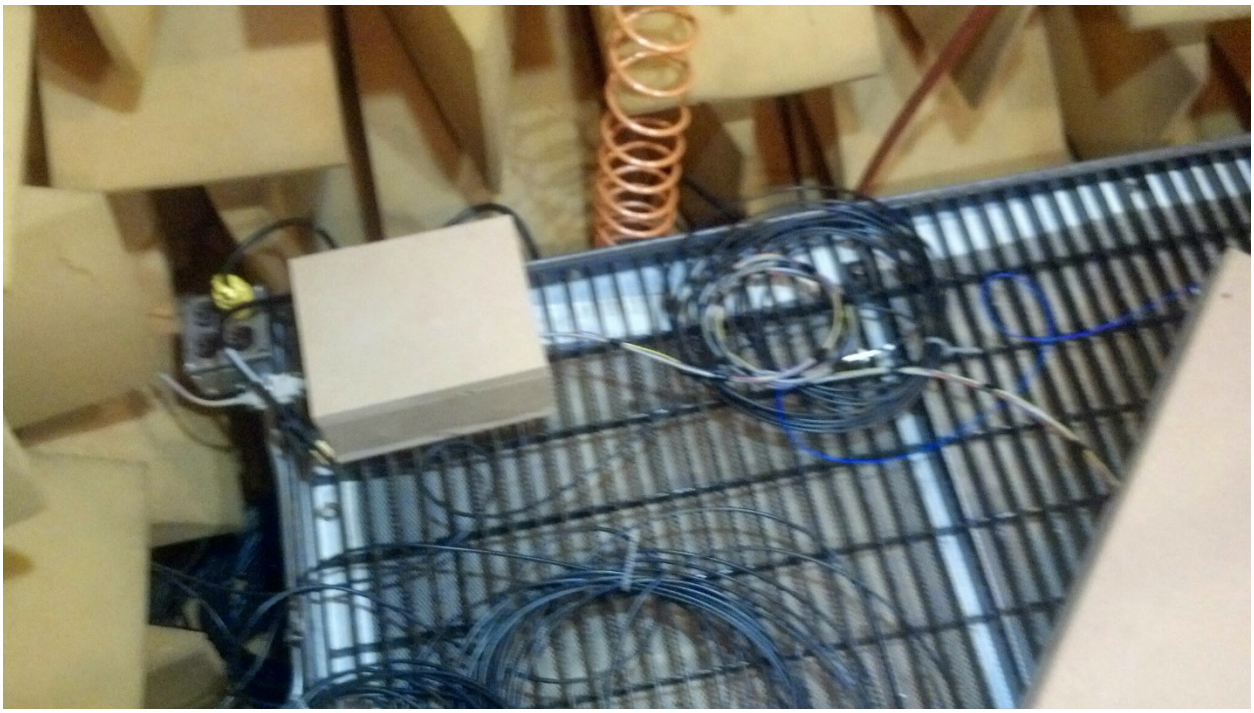

Figure A5: Cabling running from the stepper motor and encoder to the box with the driver and power supply.

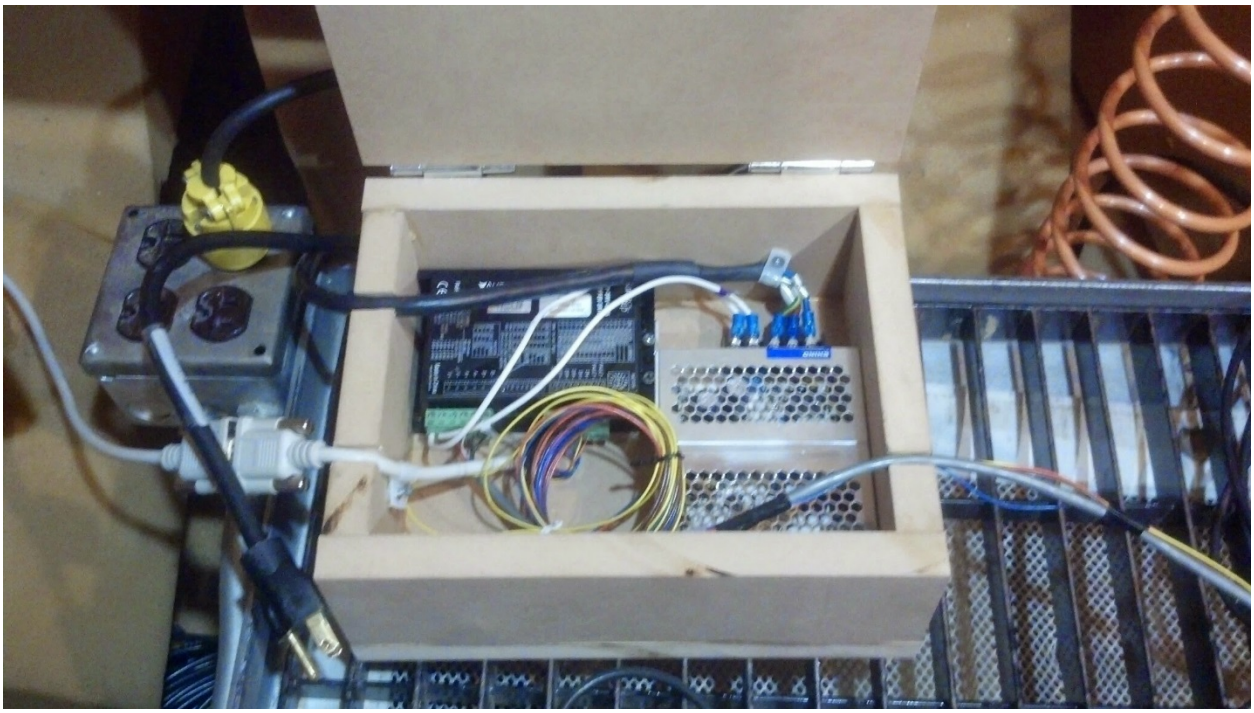

Figure A6: Inside off the box with the motor drive in the top left, power supply in the bottom right, and the white serial cable connected on the far left.

Figure A7: Outside chamber showing the power supply (left), serial cable going to the chamber in white (middle), and the cRIO with NI 9512 stepper control module (right).

Figure A8: For the CNT work, the main base was not used due to deconstructive reflections at certain frequencies. This setup mimics that used for the efficiency and THD the work presented in this report.

In order to measure the power going into the CNT thermophone a Fluke 80i-110s clamp-on current probe was used, because it can be sampled up to 100 kHz. To measure the voltage a PXIe-4497 card was used with a custom manufactured voltage attenuator. A simple voltage divider circuit can reduce voltage, but for high frequency content you also have to match the impedance of the attenuator to that of the frontend. This is what is done with oscilloscope attenuator probes. Unfortunately, the PXIe chassis has an impedance of 10 MΩ 35 pF which is different than an oscilloscope so a custom probe was designed and built with the help of Steve Lehman. Figure A9 shows the schematic. The probe could then be attached to the backside of the amplifier. While the voltages observed are a direct function of the resistance of the thermophone, typical voltage values were around 60-100 V_{pk}, much higher than the PXIe-4497 limit of 10 V_{pk}. It should be noted that an adjustable capacitor was used in the attenuator and it must be calibrated before testing. You calibrate the attenuator similar to how you calibrate an oscilloscope probe, by playing a high

frequency (15 kHz +) square wave into the attenuator and adjusting the capacitance until the square wave is square (i.e. the leading edge and trailing edge are at the same voltage).

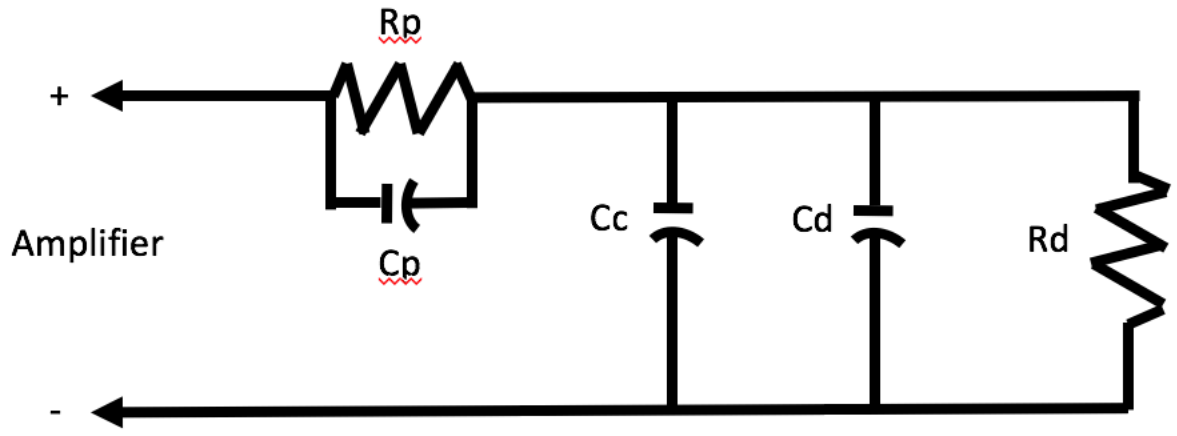

Figure A9: General schematic of custom voltage attenuator fabricated. Rp is the resistance of the custom probe, Cp is the capacitance of the probe (i.e. this is what you adjust to calibrate it), Cc is the capacitance of the short cable of the probe, Cd is the capacitance of the DAQ (35 pF), and Rd is the resistance of the DAQ (10 MΩ).

A.2 Programming/Hardware

LabVIEW was used to automate the setup. The program was created with a computer running LabVIEW connected to a cRIO-9075 connected to a NI 9512 stepper controller module. The wiring is described in Figure A10. There are two cables coming out of the 9512, one for the encoder and one for the motor. These wires were pinned out and matched up to a serial cable and a power supply outside of the chamber. The serial cable was then fed through the routing tube into the anechoic chamber. Inside the chamber a serial connector was placed to allowed for a quick disconnect inside the anechoic chamber. Inside the chamber is a MDF box with the stepper motor driver (i.e. what provides the power to the motor) and a power supply (Figure A6). The wires from the motor wire on the 9512 are connected to the stepper motor driver and the encoder wires are directly connected to the encoder. Then wires run from the MDF box to the stepper motor on the underside of the lazy-Susan assembly. When programming this setup, the drive was disabled

before acquiring acoustic data to prevent the switching frequency noise from being detected in the data.

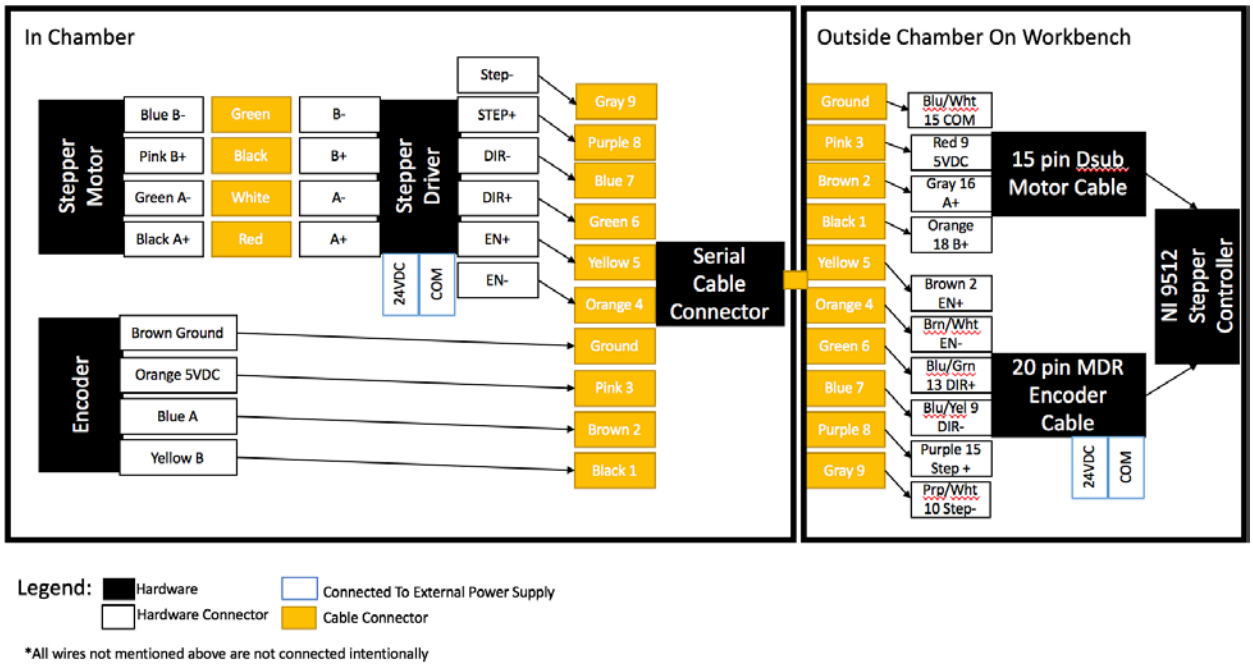

Figure A10: Wiring diagram to connect the NI 9512 module to the stepper motor driver, controller, and a power supply. Note: the power supply in the chamber and on outside on the workbench are two separate power supplies.

The NI 9074 cRIO was used in scan mode to allow for interaction with the SoftMotion features. The main VI uses a state machine architecture with use of subVIs. The states are described in Table A3.

Table A3: Program state descriptions.

State	Description
Initialize Hardware	The wav file is loaded and all channels are configured
Current Probe Calibration	The raw signal from the current probe is plotted so the user can make sure it has a mean of zero before each test
Take Data	The wav file is output and data is acquired in a producer/consumer architecture. The data is saved into FGVs
Index	The lazy-Susan rotates the specified amount
Close Hardware	The hardware was closed and the signal processing was done to get to sound power. This includes the computation of all of the correction factors.

Additional states included save and loading of the setup files. The setup files include all of the information on the “Test Setup” page as well as the “Overshoot correction” value in the “Testing” page. Inside of the Wait For User state I included a lazy-Susan return to home and save data to .mat file feature in addition to some other small features.

In operation the program functions by going from left to right in the tab structure. The first tab, Test Setup, has all of the parameters needed to complete a successful test (Figure A11). Every input box should be filled out here. The temperature and pressure can be found on the clock on the test bench. It has a wireless probe inside the chamber for the “outside” condition, i.e. the conditions in the chamber. Once ready, the user clicks the “Confirm” button. In the second tab, Current Probe Cal, there is just a plot of the raw current probe data (Figure A12). While viewing this screen, the user adjusts the knob on the current probe such that the mean is ~0 Volts. Values of +/-300E-6 Volts were acceptable. Once the user is ready to start a test, click “Complete: Start Test.” The program will automatically move the user to the “Testing” tab (Figure A13).

Once on the “Testing” tab, the user can view the raw data output to the amp at the top and the response from mic 4 and 5 on the bottom. As mentioned on the Test Setup tab, Mic 1 is directly above the source and Mic 4 is on axis. Mic 5 was a high frequency mic also on axis that was used to calculate THD. Mic 5 is not used in the sound power calculation and can just be left unplugged if unneeded. The Overshoot Correction value is an adjustment amount to get the stepper motor to move the correct distance. This will need to be adjusted if using rotation angles different than 60 degrees. The final tab, the results tab, automatically comes up once the test is complete (Figure A14). Here, at the top, sound power is shown as a function of frequency. The run number can be changed in the top left hand corner to see the response from the five different microphones during each run (e.g. if you had a 60 degree rotation then there would be 360/60=6 runs per test).

Once a test is completed, the user can click “Save” to save their data to a .mat file. After that, the user should click “Move Back” to move the lazy susan to the home position. Once there, the user can use the “Back” and “Forward” buttons to align the lazy susan perfectly with home via the webcam. The “AutoSaveSetup” and Next File “Start” buttons should only be used if you know how to edit LabVIEW. These buttons were used to programmatically load different wav files in based on their names. Manually starting a new acquisition can be done without these buttons by returning the lazy-Susan, clicking back to the “Test Setup” tab, and starting the next test that way.

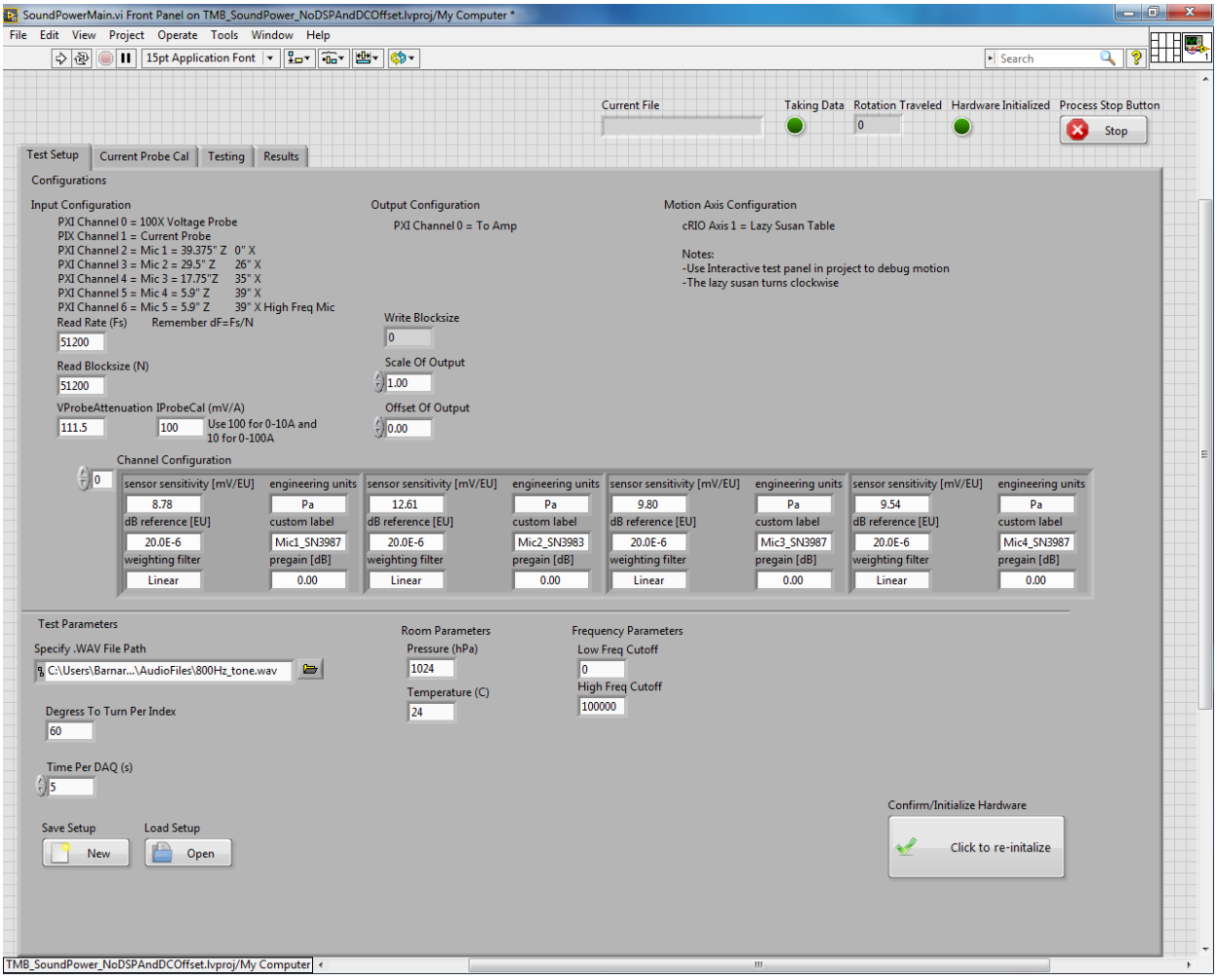

Figure A11: Test setup page. Here the user specifies all aspects of the test.

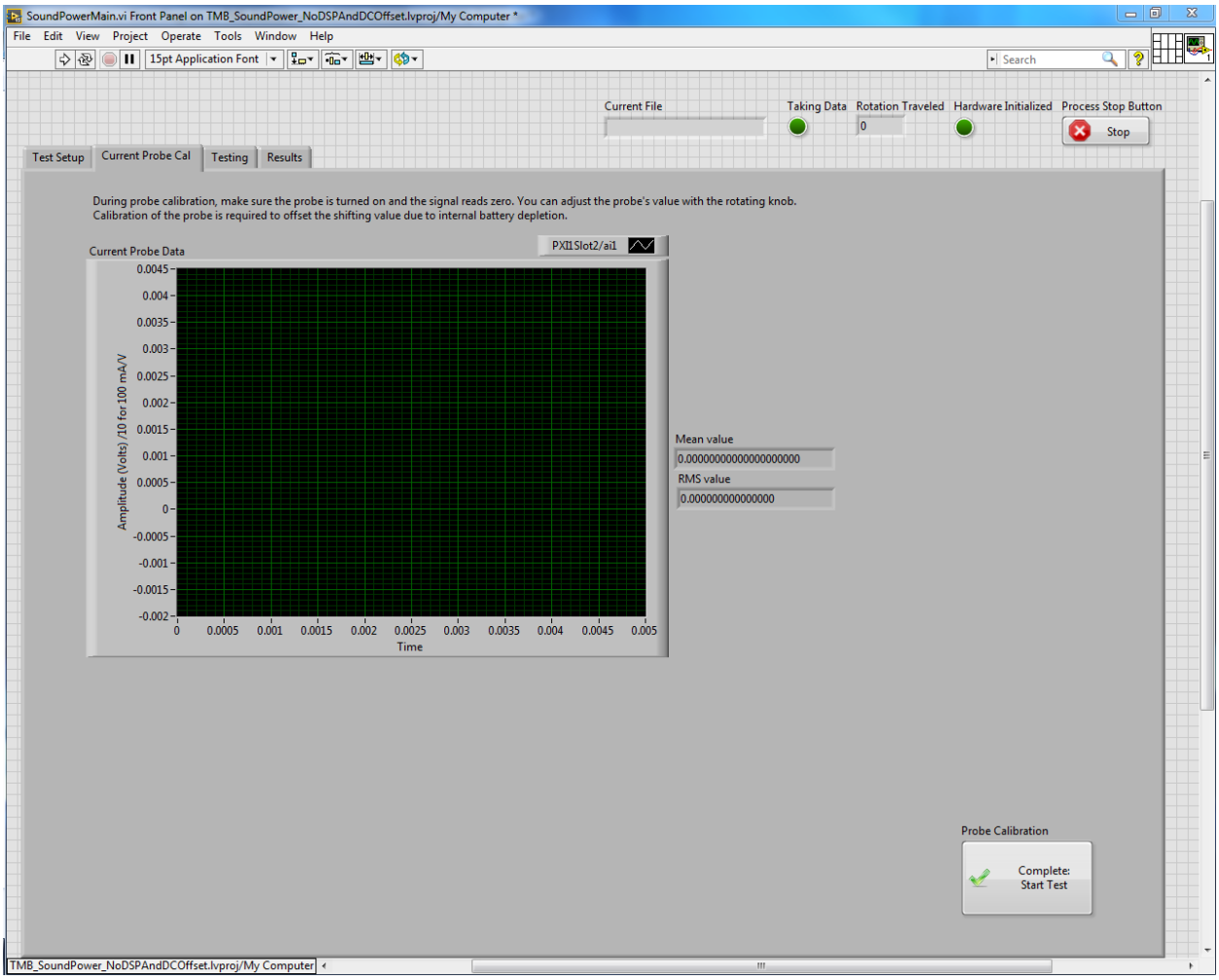

Figure A12: Current probe calibration tab. Here the user makes sure the mean of the current probe signal is ~0 Volts.

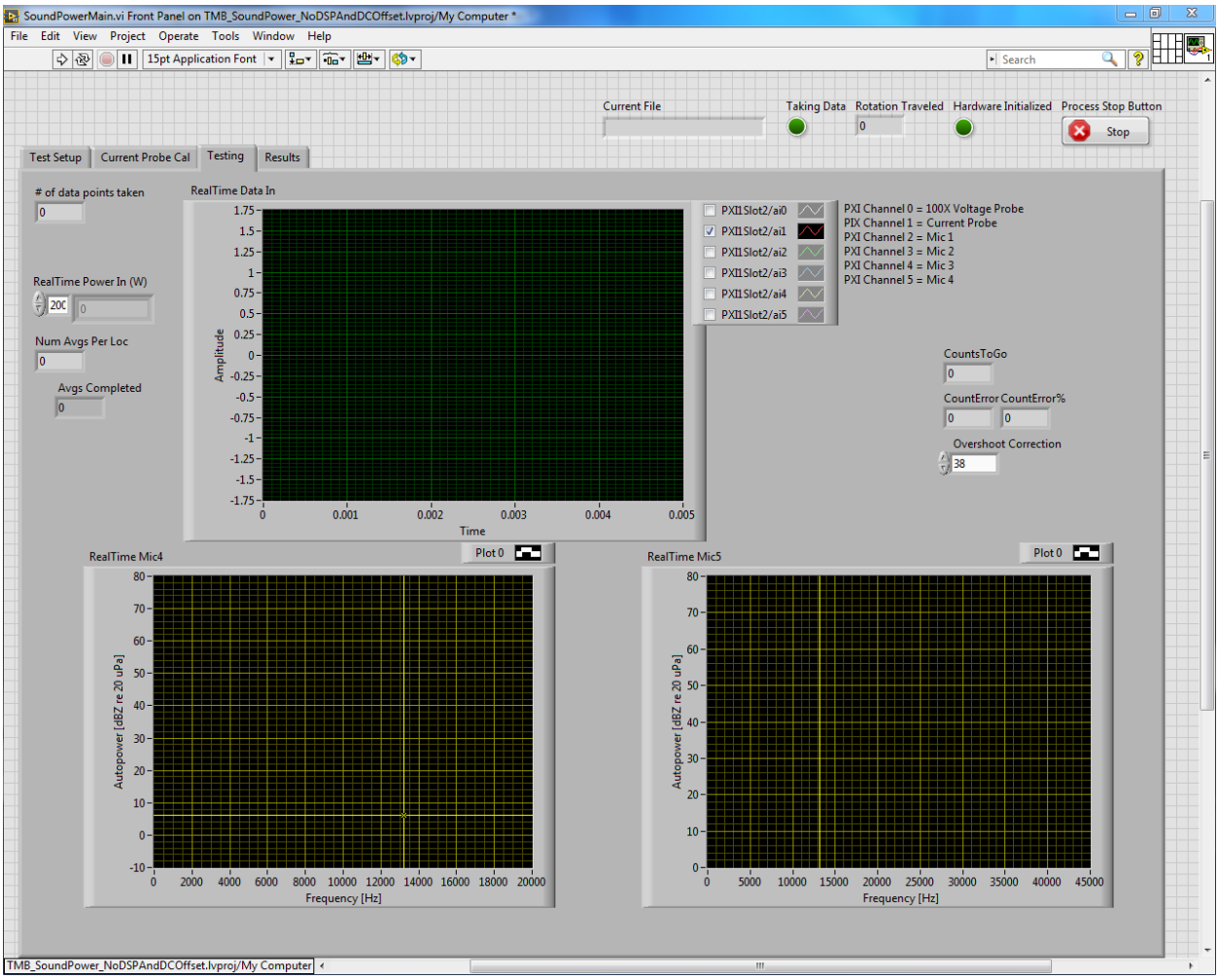

Figure A13: Testing page shows the user the current signal be output on top followed by the response from the on axis microphones at position 4 and 5.

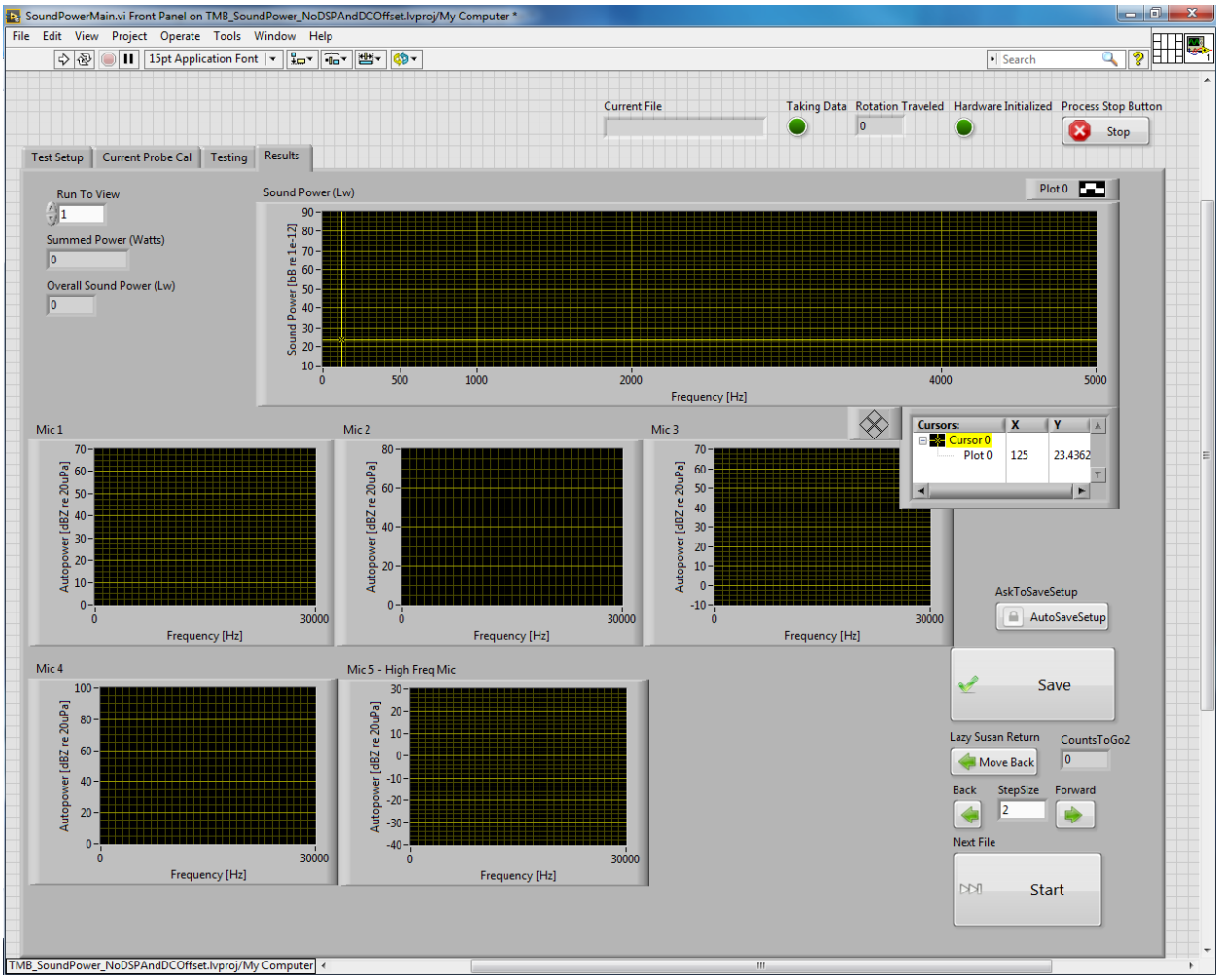

Figure A14: The Results tab shows the sound power as a function of frequency on the top followed by the microphone responses for each channel.

At the top of the screen there are indicators to assist the user (Figure A15). The first, Current File, shows the name of the wav file being played. The "Taking Data" light is illuminated at any time the program is acquiring data. The "Rotation Traveled" indicator tells the user how many degrees the lazy-Susan has traveled thus far. The "Hardware Initialized" illuminates once the DAQ has been armed. Lastly, the "Stop" button can be used to stop the program. This button should not be pressed when the stepper motor is moving, otherwise it will continue to move forever. If this happens, the "DisableTest.vi" in the Test folder can be used to disable the drive. Alternatively, the drive can also be disabled from the LabVIEW interactive test panel.

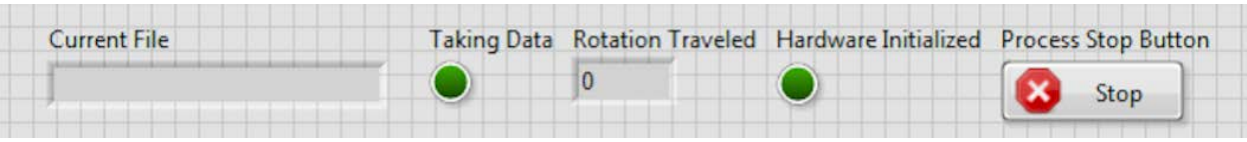

Figure A15: View of the indicators at the top of the program.

An example workspace from a saved mat file is shown in Figure A16. The current, voltage, and mics 1 thru 5 variables have the number of rows equal to the number of runs per test (e.g. in this case 6 for 60 degree rotations). The number of columns, e.g. 20480 in this case, is the number of spectral lines. The freq variable is the frequency vector for the current, voltage, and mic data. The L_W is the sound power as a function of frequency (LwFcs). The phase is the phase relationship computed from the crosspower of voltage and current for the last run. Lastly, the variable overallLw is overall sound power computed by summing the L_W variable and adjusting for amplitude and energy correction factors.

Workspace

Name	Value
current	6x20480 double
freq	20480x1 double
Lw	20001x1 double
LwFcs	20001x1 double
mic1	6x20480 double
mic2	6x20480 double
mic3	6x20480 double
mic4	6x20480 double
mic5	6x20480 double
overallLw	86.4451
phase	20480x1 double
voltage	6x20480 double
watts	6x20480 double

Figure A16: Example workspace saved from the sound power test fixture.

A.3 Validation

To validate the software, the B&K known sound source was measured and the results from the software were compared to the known values to make sure they were within 1 dB re 20μPa. The electrical side was validated by measuring a known voltage, current, and therefore power to make sure the software reported that value at a range of frequencies. The current probe was not validated as it was a purchased product. It was just adjusted before every test to make sure it did not have a DC offset, which is what happens as the 9 V battery dies. The voltage attenuator was validated with calibration of a 20 kHz square wave. After calibration, a range of known amplitudes and frequencies were applied to the attenuator and the measured values on the attenuator were used to determine its actual attenuation of 111.5x It was designed to have 100x, but due to the inherent error in the components (e.g. resistors +/-5%) and lack of specific resistors some deviation was expected.

A.4 Known issues

The only known issue is that the stepper motor only uses a simple control method using the encoder for feedback. Sometimes this results in poor angle resolution when turning. For example, you could not specify 2 degree rotations and expect it to move exactly 360 degrees for a full test. This is especially true in the summer when the MDF expands and sometimes causes the lazy-Susan to bind. A more robust control algorithm would help the program significantly, but it worked well enough for the 60 degree rotations required in the ANSI S12.54 test.